

Preconditioned Inexact Stochastic ADMM for Deep Models*

Shenglong Zhou[†] Ouya Wang[‡] Ziyang Luo[§] Yongxu Zhu[¶] Geoffrey Ye Li^{||}

Abstract: The recent advancement of foundation models (FMs) has brought about a paradigm shift, revolutionizing various sectors worldwide. The popular optimizers used to train these models are stochastic gradient descent-based algorithms, which face inherent limitations, such as slow convergence and stringent assumptions for convergence. In particular, data heterogeneity arising from distributed settings poses significant challenges to their theoretical and numerical performance. This paper develops an algorithm, PISA (**P**reconditioned **I**nexact **S**tochastic **A**lternating Direction Method of Multipliers). Grounded in rigorous theoretical guarantees, the algorithm converges under the sole assumption of Lipschitz continuity of the gradient on a bounded region, thereby removing the need for other conditions commonly imposed by stochastic methods. This capability enables the proposed algorithm to tackle the challenge of data heterogeneity effectively. Moreover, the algorithmic architecture enables scalable parallel computing and supports various preconditions, such as second-order information, second moment, and orthogonalized momentum by Newton-Schulz iterations. Incorporating the latter two preconditions in PISA yields two computationally efficient variants: SISA and NSISA. Comprehensive experimental evaluations for training or fine-tuning diverse deep models, including vision models, large language models, reinforcement learning models, generative adversarial networks, and recurrent neural networks, demonstrate superior numerical performance of SISA and NSISA compared to various state-of-the-art optimizers.

Keywords: Foundation models, SGD, preconditioned inexact stochastic ADMM, global convergence, data heterogeneity, high numerical performance

1 Introduction

Foundation models (FMs) have led to extensive applications across a variety of industries. For instance, fine-tuning large language models (LLMs), such as Gemma [70], GPT [52], and Llama [67], with user-specific data can significantly enhance the model performance. Diffusion models (DMs) are increasingly used to generate personalized content, including images, audio, and video, for entertainment. Vision models (VMs), like ResNet [23] and vision transformers (ViT) [13], are in high demand for tasks, such as image classification, segmentation, and object detection on large-scale image datasets. However, the growing complexity and scale of these tasks present

*This work was supported by the National Key R&D Program of China (2023YFA1011100), the Fundamental Research Funds for the Central Universities, the National Natural Science Foundation of China (No.12271022), and the Talent Fund of Beijing Jiaotong University (*Corresponding authors: Ouya Wang and Shenglong Zhou*).

[†]School of Mathematics and Statistics, Beijing Jiaotong University, China (shlzhou@bjtu.edu.cn).

[‡]ITP Lab, Department of EEE, Imperial College London, UK (ouya.wang20@imperial.ac.uk).

[§]School of Mathematics and Statistics, Beijing Jiaotong University, China (luozy@bjtu.edu.cn).

[¶]National Mobile Communications Research Laboratory, Southeast University, China (yongxu.zhu@seu.edu.cn).

^{||}ITP Lab, Department of EEE, Imperial College London, UK (geoffrey.li@imperial.ac.uk).

considerable challenges for widely used stochastic gradient descent (SGD)-based optimizers due to their inherent limitations. In this section, we review a subset of these methods, sufficient to motivate the development of our proposed approach.

1.1 SGD-based learning algorithms

It is known that the plain SGD-based algorithms, such as the original stochastic approximation approaches [60, 11], the parallelized SGD [98] for machine learning, and the newly developed federated averaging (FedAvg [47, 39]) and local SGD (LocalSGD [65]) algorithms for federated learning, are frequently prone to high sensitivity to poor conditioning [51] and slow convergence in high-dimensional and non-convex landscapes [10]. To overcome these drawbacks, SGD with momentum and adaptive learning rates has been proposed to enhance robustness and accelerate convergence. The former introduced first-order momentum to suppress the oscillation of SGD [56], and the latter updated the learning rate iteratively based on historical information.

For instance, the adaptive gradient (AdaGrad [16]) interpolated the accumulated second-order moment of gradients to achieve the adaptive learning rate. The root mean-squared propagation (RMSProp [68]) exploited an exponential weighting technique to balance the distant historical information and the knowledge of the current second-order gradients, avoiding premature termination encountered by AdaGrad. The adaptive moment (Adam [31]) combined the first-order moment and adaptive learning rates, thereby exhibiting robustness to hyperparameters. Adaptive method setup based gradient (AMSGrad [59]) took smaller learning rates than those of Adam by using a maximum value for normalizing the running average of the gradients, thereby fixing the convergence of Adam. Partially Adam (Padam [9]) employed a similar strategy of AMSGrad with the difference of the rate power. Adam with dynamic bounds on learning rates (AdaBound [44]) designed a clipping mechanism on Adam-type learning rates by clipping the gradients larger than a threshold to avoid gradient explosion. Parallel restarted SGD (PRSGD [85]) simply benefited from a decayed power learning rate. A layerwise adaptive large batch optimization technique (Lamb [84]) performed per dimension normalization with respect to the square root of the second moment used in Adam and set large batch sizes suggested by the layerwise adaptive rate scaling method (Lars [83]).

For some other SGD-based algorithms, one can refer to a per-dimension learning rate method based gradient descent (AdaDelta [87]), a variant of Adam based on the infinity norm (Adamax [31]), Adam with decoupled weight decay (AdamW [43]), a structure-aware preconditioning algorithm (Shampoo [22]), momentum orthogonalized by Newton-Schulz iterations (Muon [29]), Shampoo with Adam in the preconditioner’s eigenbasis (SOAP [73]), Adam with fewer learning rates (Adam-mini [93]), and those reviewed in nice surveys [6, 62, 7].

The aforementioned algorithms primarily leveraged the heavy ball acceleration technique to estimate the first- and second-order moments of the gradient. An alternative approach for accelerating convergence is Nesterov acceleration, which has been theoretically proven to converge faster [49, 50]. This has led to the development of several Nesterov-accelerated SGD algorithms. For example, Nesterov-accelerated Adam (NAdam [14]) integrated this technique into Adam to enhance

convergence speed. More recently, an adaptive Nesterov momentum algorithm (Adan [78]) adopted Nesterov momentum estimation to refine the estimation of the first- and second-order moments of the gradient, thereby improving adaptive learning rate adjustments for faster convergence.

1.2 ADMM-based learning algorithms

The alternating direction method of multipliers (ADMM) [19, 8] is a promising framework for solving large-scale optimization problems because it decomposes complex problems into smaller and more manageable sub-problems. This characteristic makes ADMM particularly well-suited for various challenges in distributed learning. It has demonstrated substantial potential in applications, such as image compressive sensing [80], federated learning [92, 95, 96], reinforcement learning [79], and few-shot learning [76]. It is worth noting that there are many other distributed optimization frameworks, such as dual averaging [1, 17, 26], push-sum [72], and push-pull [55]. However, in the sequel, our focus is on the family of distributed algorithms, ADMM, as they are most directly relevant to the design and convergence analysis of our algorithm.

When applied to deep model training, early studies first relaxed optimization models before developing ADMM-based algorithms. Therefore, these methods can be classified as model-driven/model-specific approaches. They targeted the relaxations rather than the original problems, enabling better handling of the challenges associated with highly non-convex optimization landscapes. For instance, an ADMM-based algorithm in [66] addressed a penalized formulation, avoiding pitfalls that hinder gradient-based methods in non-convex settings. Similarly, a deep learning ADMM algorithm [75] and its variant [18] were designed to enhance convergence by addressing penalization models as well. Moreover, the sigmoid-ADMM algorithm [88] utilized the algorithmic gradient-free property to address saturation issues with sigmoid activation functions.

Despite their advantages, model-driven ADMM approaches face two critical issues. Firstly, these algorithms exhibit high computational complexity because they require computing full gradients using the entire dataset and performing matrix inversions for weight updates, making them impractical for large-scale tasks. Additionally, the reliance on the specific structure of optimization models limits their general applicability, as different deep models often necessitate distinct formulations.

To address the aforementioned limitations, data-driven ADMM algorithms have emerged as a promising alternative, aiming to reduce computational burdens and enhance adaptability to diverse tasks. For instance, the deterministic ADMM [95, 96], designed for distributed learning problems, achieved high accuracy but low computational efficiency due to the use of full dataset gradients. Stochastic ADMM (SADMM) methods tackled the inefficiency by replacing full gradients with stochastic approximations. Examples like stochastic ADMM (S-ADMM [53]) and distributed stochastic ADMM (PS-ADMM [12]) aimed to solve sub-problems exactly and thus still involved high computational costs.

To further enhance convergence and reduce stochastic gradient variance, advanced techniques of variance reduction and Nesterov acceleration have been incorporated into SADMM. Representatives consist of stochastic average ADMM [94], stochastic path-integrated differential estimator based

ADMM (SPIDER-ADMM [27]), and accelerated stochastic variance reduced gradient based ADMM (ASVRG-ADMM) for convex [42] and non-convex problems [89]. However, these enhanced methods still relied on access to full gradients for the aim of reducing stochastic gradient variance, posing challenges for large-scale applications.

1.3 Contributions

In this work, we propose a data-driven preconditioned inexact SADMM algorithm, termed as PISA. It distinguishes itself from prior approaches and aims to reduce computational costs, relax convergence assumptions, and enhance numerical performance. The key contributions are threefold.

a) A general algorithmic structure. The algorithm is based on a preconditioned inexact SADMM, combining simplicity with high generality to handle a wide range of deep learning applications. First, the use of preconditioning matrices allows us to incorporate various forms of useful information, such as first- and second-moment (yielding SISA, a variant of PISA), second-order information (e.g., the Hessian), and orthogonalized momentum by Newton-Schulz iterations (leading to NSISA, another variant of PISA), into the updates, thereby enhancing the performance of the proposed algorithms. Moreover, the proposed algorithmic framework is inherently compatible with parallel computing, making it ideal for large-scale data settings.

b) Strong convergence theory under a sole assumption. PISA is proven to converge under a single assumption: the Lipschitz continuity of the gradient. Despite relying on stochastic gradients, it avoids many of the assumptions typically required by stochastic algorithms. As highlighted in Table 1, all algorithms, except for PISA and FedAvg [39], have drawn identically and independently distributed (IID) samples to derive stochastic gradients for unbiased gradient estimation. However, real-world data are often heterogeneous (i.e., non-IID), a phenomenon commonly referred to as statistical or data heterogeneity [38, 30, 37, 81], which poses significant challenges to the convergence of these algorithms for IID datasets.

Additionally, the table also presents the algorithmic convexity of two types of convergence. Type I convergence, $F(\mathbf{w}^T) - F^* = B$, refers to a rate B at which objective values $\{F(\mathbf{w}^T)\}$ of generated sequence $\{\mathbf{w}^T\}$ approach F^* , where T is the number of iterations and F^* is the limit of sequence $\{F(\mathbf{w}^T)\}$ or a function value at a stationary point. For instance, $B = O(1/T)$ indicates a sublinear convergence, while $B = O(\gamma^T)$ with $\gamma \in (0, 1)$ implies a linear rate. Type II convergence describes how quickly the length, $\{\|\nabla F(\mathbf{w}^T)\|\}$, of gradients diminishes, reflecting the stationarity of the iterates. Therefore, ASVRG-ADMM [42] and PISA achieve the best Type I convergence rate. However, the former imposes several restrictive assumptions, while PISA requires a single assumption (i.e., ②). We emphasize that condition ② is closely related to the locally Lipschitz continuity of the gradient, which is a mild assumption. It is weaker than ③, and any twice continuously differentiable function satisfies ②. More importantly, we eliminate the need for conditions on the boundedness of the stochastic gradient, the second moment of the stochastic gradient, and variance. This makes PISA well-suited for addressing the challenges associated with data heterogeneity, an open problem in federated learning [30, 81].

c) *High numerical performance for various applications.* The effectiveness of PISA and its two variants, SISA and NSISA, is demonstrated through comparisons with many state-of-the-art optimizers using several deep models: VMs, LLMs, reinforcement learning models (RLMs), generative adversarial networks (GANs), and recurrent neural networks (RNNs), highlighting its great potential for extensive applications. In particular, numerical experiments on heterogeneous datasets corroborate our claim that PISA effectively addresses this challenge.

Table 1: Assumptions imposed by different stochastic algorithms for convergence: ①: Convexity; ②: Strong convexity; ③: Lipschitz continuity of the gradient; ④: Bounded (stochastic) gradient or the second-moment of the (stochastic) gradient; ⑤: Bounded variance; ⑥: Bounded sequence generated by the algorithm; ⑦: Unbiased gradient estimation; ⑧: Compact convex feasible region; ⑨: Lipschitz continuity of the objective function; ⑩: Lipschitz sub-minimization paths; ⑪: Bounded dual variables; ⑫: Lipschitz continuity of the gradient on a bounded region.

Algorithms	Refs.	Class	Data	Convergence rate B	Assumptions
Type I convergence: $F(\mathbf{w}^T) - F^* = B$					
AdaGrad	[16]	SGD	IID	$O(1/\sqrt{T})$	①④⑥
Adam	[31]	SGD	IID	$O(1/\sqrt{T})$	①④⑥
RMSProp	[48]	SGD	IID	$O(1/\sqrt{T})$	①④⑥
AMSGrad	[59]	SGD	IID	$O(1/\sqrt{T})$	①④⑧
AdaBound	[44]	SGD	IID	$O(1/\sqrt{T})$	①④⑧
FedAvg	[39]	SGD	IID/Non-IID	$O(1/T)$	②③④⑤
LocalSGD	[65]	SGD	IID	$O(1/T)$	②③④⑤
S-ADMM	[53]	SADMM	IID	$O(\log(T)/T)$	②④⑧
ASVRG-ADMM	[42]	SADMM	IID	$O(1/T^2)$	①③⑧⑩
ASVRG-ADMM	[42]	SADMM	IID	$O(\gamma^T)$	②③⑧⑩
PS-ADMM	[12]	SADMM	IID	$O(1/T)$	②③⑨
PISA	Ours	SADMM	IID/Non-IID	$O(\gamma^T)$	⑫
Type II convergence: $\ \nabla F(\mathbf{w}^T)\ ^2 = B$					
Adam	[99]	SGD	IID	$O(\log(T)/\sqrt{T})$	③④⑦
Padam	[9]	SGD	IID	$O(1/\sqrt{T})$	③④⑦
PRSGD	[85]	SGD	IID	$O(1/\sqrt{T})$	③④⑤⑦
Lamb	[84]	SGD	IID	$O(1/\sqrt{T})$	③④⑤
Adan	[78]	SGD	IID	$O(1/\sqrt{T})$	③④⑤⑦
FedAvg	[58]	SGD	IID/Non-IID	$O(1/\sqrt{T})$	③④⑤⑦
SPIDER-ADMM	[27]	SADMM	IID	$O(1/T)$	③④

1.4 Organization and Notation

The paper is organized as follows: In the next section, we introduce the main model and develop the proposed algorithm, PISA. Section 3 provides rigorous proofs of the convergence. Section 4.2 specifies the pre-condition by the second moment to derive a variation of PISA, termed as SISA (second-moment-based inexact SADMM). Extensive experimental results validating the effectiveness of SISA are provided in Section 5. Concluding remarks are discussed in the last section.

Throughout the paper, let $[m] := \{1, 2, \dots, m\}$, where ‘:=’ means ‘define’. The cardinality of a set \mathcal{D} is written as $|\mathcal{D}|$. For two vectors \mathbf{w} and \mathbf{v} , their inner product is denoted by $\langle \mathbf{w}, \mathbf{v} \rangle := \sum_i w_i v_i$. Let $\|\cdot\|$ be the Euclidean norm for vectors, namely $\|\mathbf{w}\| = \sqrt{\langle \mathbf{w}, \mathbf{w} \rangle}$, and the Spectral norm for matrices. A ball with a positive radius r is written as $\mathbb{N}(r) := \{\mathbf{w} : \|\mathbf{w}\| \leq r\}$. A symmetric positive semi-definite matrix \mathbf{Q} is written as $\mathbf{Q} \succeq 0$. Then $\mathbf{P} \succeq \mathbf{Q}$ means that $\mathbf{P} - \mathbf{Q} \succeq 0$. Denote the identity matrix by \mathbf{I} and let $\mathbf{1}$ be the vector with all entries being 1. We write

$$\begin{aligned} \mathbf{\Pi} &= (\boldsymbol{\pi}_1, \boldsymbol{\pi}_2, \dots, \boldsymbol{\pi}_m), & \mathbf{W} &= (\mathbf{w}_1, \mathbf{w}_2, \dots, \mathbf{w}_m), \\ \mathbf{M} &= (\mathbf{m}_1, \mathbf{m}_2, \dots, \mathbf{m}_m), & \boldsymbol{\sigma} &= (\sigma_1, \sigma_2, \dots, \sigma_m). \end{aligned}$$

Similar rules are also employed for the definitions of $\mathbf{\Pi}^\ell$, \mathbf{W}^ℓ , \mathbf{M}^ℓ , and $\boldsymbol{\sigma}^\ell$.

2 Preconditioned Inexact SADMM

We begin this section by introducing the mathematical optimization model for general distributed learning. Then we go through the development of the algorithm.

2.1 Model description

Suppose we are given a set of data as $\mathcal{D} := \{\mathbf{x}_t : t = 1, 2, \dots, |\mathcal{D}|\}$, where \mathbf{x}_t is the t th sample. Let $f(\mathbf{w}; \mathbf{x}_t)$ be a function (such as neural networks) parameterized by \mathbf{w} and sampled by \mathbf{x}_t . The total loss function on \mathcal{D} is defined by $\sum_{\mathbf{x}_t \in \mathcal{D}} f(\mathbf{w}; \mathbf{x}_t) / |\mathcal{D}|$. We then divide data \mathcal{D} into m disjoint batches, namely, $\mathcal{D} = \mathcal{D}_1 \cup \mathcal{D}_2 \cup \dots \cup \mathcal{D}_m$ and $\mathcal{D}_i \cap \mathcal{D}_{i'} = \emptyset$ for any two distinct i and i' . Denote

$$H_i(\mathbf{w}; \mathcal{D}_i) := \frac{1}{|\mathcal{D}_i|} \sum_{\mathbf{x}_t \in \mathcal{D}_i} f(\mathbf{w}; \mathbf{x}_t) \quad \text{and} \quad \alpha_i := \frac{|\mathcal{D}_i|}{|\mathcal{D}|}. \quad (2.1)$$

Clearly, $\sum_{i=1}^m \alpha_i = 1$. Now, we can rewrite the total loss as follows,

$$\frac{1}{|\mathcal{D}|} \sum_{\mathbf{x}_t \in \mathcal{D}} f(\mathbf{w}; \mathbf{x}_t) = \frac{1}{|\mathcal{D}|} \sum_{i=1}^m \sum_{\mathbf{x}_t \in \mathcal{D}_i} f(\mathbf{w}; \mathbf{x}_t) = \sum_{i=1}^m \alpha_i H_i(\mathbf{w}; \mathcal{D}_i).$$

The task is to learn an optimal parameter to minimize the following regularized loss function,

$$\min_{\mathbf{w}} \sum_{i=1}^m \alpha_i H_i(\mathbf{w}; \mathcal{D}_i) + \frac{\mu}{2} \|\mathbf{w}\|^2, \quad (2.2)$$

where $\mu \geq 0$ is a penalty constant and $\|\mathbf{w}\|^2$ is a regularization.

2.2 Main model

Throughout the paper, we focus on the following equivalent model of problem (2.2),

$$F^* := \min_{\mathbf{w}, \mathbf{W}} \sum_{i=1}^m \alpha_i F_i(\mathbf{w}_i) + \frac{\lambda}{2} \|\mathbf{w}\|^2, \quad \text{s.t. } \mathbf{w}_i = \mathbf{w}, \quad i \in [m], \quad (2.3)$$

where $\lambda \in [0, \mu]$ and

$$\begin{aligned} F_i(\mathbf{w}) &:= F_i(\mathbf{w}; \mathcal{D}_i) := H_i(\mathbf{w}; \mathcal{D}_i) + \frac{\mu - \lambda}{2} \|\mathbf{w}\|^2, \\ F(\mathbf{w}) &:= \sum_{i=1}^m \alpha_i F_i(\mathbf{w}), \quad F_\lambda(\mathbf{w}) := F(\mathbf{w}) + \frac{\lambda}{2} \|\mathbf{w}\|^2. \end{aligned} \quad (2.4)$$

In problem (2.3), m auxiliary variables \mathbf{w}_i are introduced in addition to the global parameter \mathbf{w} . We emphasize that problems (2.2) and (2.3) are equivalent in terms of their optimal solutions but are expressed in different forms when $\lambda \in [0, \mu)$, and they are identical when $\lambda = \mu$. Throughout this work, we assume that optimal function value F^* is bounded from below. It is worth noting that any stationary point \mathbf{w} of problem (2.3) satisfies

$$0 \in \nabla F_\lambda(\mathbf{w}) = \sum_{i=1}^m \alpha_i \nabla F_i(\mathbf{w}) + \lambda \mathbf{w}, \quad (2.5)$$

where $\nabla F_i(\mathbf{w})$ is the sub-differential [61, Definition 8.3] of $F_i(\mathbf{w})$. In our convergence analysis, we assume that F_i is continuously differentiable, so sub-differential $\nabla F_i(\mathbf{w})$ reduces to the gradient of $F_i(\mathbf{w})$. In this case, inclusion ‘ \in ’ reduces to ‘ $=$ ’. Moreover, if each F_i is convex (which is unnecessary in this paper), then the stationary points coincide with the optimal solutions to (2.3). Since problems (2.3) and (2.2) are equivalent, their stationary points are also identical.

2.3 The algorithmic design

When employing ADMM to solve problem (2.3), we need its associated augmented Lagrange function, which is defined as follows,

$$\begin{aligned} \mathcal{L}(\mathbf{w}, \mathbf{W}, \mathbf{\Pi}; \boldsymbol{\sigma}) &:= \sum_{i=1}^m \alpha_i L_i(\mathbf{w}, \mathbf{w}_i, \boldsymbol{\pi}_i; \sigma_i) + \frac{\lambda}{2} \|\mathbf{w}\|^2, \\ L_i(\mathbf{w}, \mathbf{w}_i, \boldsymbol{\pi}_i; \sigma_i) &:= F_i(\mathbf{w}_i) + \langle \boldsymbol{\pi}_i, \mathbf{w}_i - \mathbf{w} \rangle + \frac{\sigma_i}{2} \|\mathbf{w}_i - \mathbf{w}\|^2, \end{aligned} \quad (2.6)$$

where $\sigma_i > 0$ and $\boldsymbol{\pi}_i, i \in [m]$ are the Lagrange multipliers. Based on the above augmented Lagrange function, the conventional ADMM updates each variable in $(\mathbf{w}, \mathbf{W}, \mathbf{\Pi})$ iteratively. However, we modified the framework as follows. Given initial point $(\mathbf{w}^0, \mathbf{W}^0, \mathbf{\Pi}^0; \boldsymbol{\sigma}^0)$, the algorithm performs the following steps iteratively for $\ell = 0, 1, 2, \dots$,

$$\mathbf{w}^{\ell+1} = \arg \min_{\mathbf{w}} \mathcal{L}(\mathbf{w}, \mathbf{W}^\ell, \mathbf{\Pi}^\ell; \boldsymbol{\sigma}^\ell), \quad (2.7a)$$

$$\mathbf{w}_i^{\ell+1} = \arg \min_{\mathbf{w}_i} L_i(\mathbf{w}^{\ell+1}, \mathbf{w}_i, \boldsymbol{\pi}_i^\ell; \sigma_i^{\ell+1}) + \frac{\rho_i}{2} \left\langle \mathbf{w}_i - \mathbf{w}^{\ell+1}, \mathbf{Q}_i^{\ell+1} (\mathbf{w}_i - \mathbf{w}^{\ell+1}) \right\rangle, \quad (2.7b)$$

$$\boldsymbol{\pi}_i^{\ell+1} = \boldsymbol{\pi}_i^\ell + \sigma_i^{\ell+1} (\mathbf{w}_i^{\ell+1} - \mathbf{w}^{\ell+1}), \quad (2.7c)$$

Algorithm 1: Preconditioned Inexact Stochastic ADMM (PISA).

Divide \mathcal{D} into m disjoint batches $\{\mathcal{D}_1, \mathcal{D}_2, \dots, \mathcal{D}_m\}$ and calculate α_i by (2.1).

Initialize $\mathbf{w}^0 = \mathbf{w}_i^0 = \boldsymbol{\pi}_i^0 = 0$, $\gamma_i \in [3/4, 1)$, and $(\sigma_i^0, \eta_i, \rho_i) > 0$ for each $i \in [m]$.

for $\ell = 0, 1, 2, \dots$ **do**

$$\mathbf{w}^{\ell+1} = \frac{\sum_{i=1}^m \alpha_i (\sigma_i^\ell \mathbf{w}_i^\ell + \boldsymbol{\pi}_i^\ell)}{\sum_{i=1}^m \alpha_i \sigma_i^\ell + \lambda}. \quad (2.9)$$

for $i = 1, 2, \dots, m$ **do**

Randomly draw a mini-batch $\mathcal{B}_i^{\ell+1} \in \mathcal{D}_i$ and calculate $\mathbf{g}_i^{\ell+1} = \nabla F_i(\mathbf{w}^{\ell+1}; \mathcal{B}_i^{\ell+1})$. (2.10)

Choose $\mathbf{Q}_i^{\ell+1}$ to satisfy $\eta_i \mathbf{I} \succeq \mathbf{Q}_i^{\ell+1} \succeq 0$. (2.11)

$\sigma_i^{\ell+1} = \sigma_i^\ell / \gamma_i$. (2.12)

$\mathbf{w}_i^{\ell+1} = \mathbf{w}^{\ell+1} - \left(\sigma_i^{\ell+1} \mathbf{I} + \rho_i \mathbf{Q}_i^{\ell+1} \right)^{-1} \left(\boldsymbol{\pi}_i^\ell + \mathbf{g}_i^{\ell+1} \right)$. (2.13)

$\boldsymbol{\pi}_i^{\ell+1} = \boldsymbol{\pi}_i^\ell + \sigma_i^{\ell+1} (\mathbf{w}_i^{\ell+1} - \mathbf{w}^{\ell+1})$. (2.14)

end

end

for each $i \in [m]$, where $\rho_i > 0$, both scalar $\sigma_i^{\ell+1}$ and matrix $\mathbf{Q}_i^{\ell+1} \succeq 0$ will be updated properly. Hereafter, superscripts ℓ and $\ell + 1$ in σ_i^ℓ and $\sigma_i^{\ell+1}$ stand for the iteration number rather than the power. Here, $\mathbf{Q}_i^{\ell+1}$ is commonly referred to as an (adaptively) preconditioning matrix in preconditioned gradient methods [40, 22, 2, 82].

Remark 2.1. *The primary distinction between algorithmic framework (2.7) and conventional ADMM lies in the inclusion of a term $\frac{\rho_i}{2} \langle \mathbf{w}_i - \mathbf{w}^{\ell+1}, \mathbf{Q}_i^{\ell+1} (\mathbf{w}_i - \mathbf{w}^{\ell+1}) \rangle$. This term enables the incorporation of various forms of useful information, such as second-moment, second-order information (e.g., Hessian), and orthogonalized momentum by Newton-Schulz iterations, thereby enhancing the performance of the proposed algorithms; see Section 4.2 for more details.*

One can check that sub-problem (2.7a) admits a closed-form solution outlined in (2.9). For sub-problem (2.7b), to accelerate the computational speed, we solve it inexactly by

$$\begin{aligned} \mathbf{w}_i^{\ell+1} &= \arg \min_{\mathbf{w}_i} \langle \boldsymbol{\pi}_i^\ell, \mathbf{w}_i - \mathbf{w}^{\ell+1} \rangle + \frac{\sigma_i^{\ell+1}}{2} \|\mathbf{w}_i - \mathbf{w}^{\ell+1}\|^2 \\ &\quad + F_i(\mathbf{w}^{\ell+1}) + \langle \nabla F_i(\mathbf{w}^{\ell+1}; \mathcal{B}_i^{\ell+1}), \mathbf{w}_i - \mathbf{w}^{\ell+1} \rangle + \frac{\rho_i}{2} \left\langle \mathbf{w}_i - \mathbf{w}^{\ell+1}, \mathbf{Q}_i^{\ell+1} \left(\mathbf{w}_i - \mathbf{w}^{\ell+1} \right) \right\rangle \\ &= \mathbf{w}^{\ell+1} - \left(\sigma_i^{\ell+1} \mathbf{I} + \rho_i \mathbf{Q}_i^{\ell+1} \right)^{-1} \left(\boldsymbol{\pi}_i^\ell + \nabla F_i(\mathbf{w}^{\ell+1}; \mathcal{B}_i^{\ell+1}) \right). \end{aligned} \quad (2.8)$$

This update admits three advantages. First, it solves problem (2.7b) by a closed-form solution, namely, the second equation in (2.8), reducing the computational complexity. Second, we approximate $F_i(\mathbf{w})$ using its first-order approximation at $\mathbf{w}^{\ell+1}$ rather than \mathbf{w}_i^ℓ , which facilitates each

batch parameter $\mathbf{w}_i^{\ell+1}$ to tend to $\mathbf{w}^{\ell+1}$ quickly, thereby accelerating the overall convergence. Finally, $\nabla F_i(\mathbf{w}^{\ell+1}; \mathcal{B}_i^{\ell+1})$ serves as a stochastic approximation of true gradient $\nabla F_i(\mathbf{w}^{\ell+1}) = \nabla F_i(\mathbf{w}^{\ell+1}; \mathcal{D}_i)$, as defined by (2.4), where $\mathcal{B}_i^{\ell+1}$ is a random sample from \mathcal{D}_i . By using sub-batch datasets $\{\mathcal{B}_1^{\ell+1}, \dots, \mathcal{B}_m^{\ell+1}\}$ in every iteration, rather than full data $\mathcal{D} = \{\mathcal{D}_1, \dots, \mathcal{D}_m\}$, the computational cost is significantly reduced. Overall, based on these observations, we name our algorithm PISA, which stands for Preconditioned Inexact SADMM, as described in Algorithm 1.

Another advantageous property of PISA is its ability to perform parallel computation, which stems from the parallelism used in solving sub-problems in ADMM. At each iteration, m nodes (i.e., $i = 1, 2, \dots, m$) update their parameters by (2.10)-(2.14) in parallel, thereby enabling the processing of large-scale datasets. Moreover, when specifying the preconditioning matrix, $\mathbf{Q}_i^{\ell+1}$, as a diagonal matrix (as outlined in Section 4.2) and sampling $\mathcal{B}_i^{\ell+1}$ with small batch sizes, each node exhibits significantly low-computational complexity, facilitating fast computation.

3 Convergence of PISA

In this subsection, we aim to establish the convergence property of Algorithm 1. To proceed with that, we first define a critical bound by

$$\varepsilon_i(r) := \sup_{\mathcal{B}_i, \mathcal{B}'_i \subseteq \mathcal{D}_i, \mathbf{w} \in \mathbb{N}(r)} 64 \|\nabla F_i(\mathbf{w}; \mathcal{B}_i) - \nabla F_i(\mathbf{w}; \mathcal{B}'_i)\|^2, \quad \forall i \in [m]. \quad (3.1)$$

Lemma 3.1. $\varepsilon_i(r) < \infty$ for any given $r \in (0, \infty)$ and any $i \in [m]$.

Proof. As F_i is continuously differentiable, ∇F_i is continuous. We note that $\mathbb{N}(r)$ is bounded due to $r \in (0, \infty)$, thereby gap $\|\nabla F_i(\mathbf{w}; \mathcal{B}_i) - \nabla F_i(\mathbf{w}; \mathcal{B}'_i)\|^2$ is bounded for fixed \mathcal{B}_i and \mathcal{B}'_i . Then there are finitely many \mathcal{B}_i and \mathcal{B}'_i in \mathcal{D}_i , indicating $\varepsilon_i(r)$ is bounded. \square

One can observe that $\varepsilon_i(r) = 0$ for any $r > 0$ if we take the full batch data in each step, namely, choosing $\mathcal{B}_i^\ell = (\mathcal{B}'_i)^\ell = \mathcal{D}_i$ for every $i \in [m]$ and all $\ell \geq 1$. However for min-batch dataset $\mathcal{B}_i^\ell \subset \mathcal{D}_i$, this parameter is related to the bound of variance $\mathbb{E} \|\nabla F_i(\mathbf{w}; \mathcal{B}_i) - \nabla F_i(\mathbf{w}; \mathcal{D}_i)\|^2$, which is commonly assumed to be bounded for any \mathbf{w} [65, 85, 39, 74, 78]. However, in the subsequent analysis, we can verify that both generated sequences $\{\mathbf{w}^\ell\}$ and $\{\mathbf{w}'_i^\ell\}$ fall into a bounded region $\mathbb{N}(\delta)$ for any $i \in [m]$ with δ defined as (3.3), thereby leading to a finitely bounded $\varepsilon_i(\delta)$ naturally, see Lemma 3.2. In other words, we no longer need to assume the boundedness of the variance, $\mathbb{E} \|\nabla F_i(\mathbf{w}; \mathcal{B}_i) - \nabla F_i(\mathbf{w}; \mathcal{D}_i)\|^2$ for any \mathbf{w} . This assumption is known to be somewhat restrictive, particularly for non-IID or heterogeneous datasets. Therefore, the theorems we establish in the sequel effectively address this critical challenge [30, 81]. Therefore, our algorithm demonstrates robust performance in settings with heterogeneous data.

3.1 Convergence analysis

To establish convergence, we assume function f has a Lipschitz continuous gradient on a bounded region, namely, the gradient is locally Lipschitz continuous. This is a relatively mild condition.

Functions with (global) Lipschitz continuity and twice continuously differentiable functions satisfy this condition. It is known that the Lipschitz continuity of the gradient is commonly referred to as L-smoothness. Therefore, our assumption can be regarded as L-smoothness on a bounded region, which is weaker than L-smoothness.

Assumption 3.1. For each $t \in \llbracket \mathcal{D} \rrbracket$, gradient $\nabla f(\cdot; \mathbf{x}_t)$ is Lipschitz continuous with a constant $c(\mathbf{x}_t) > 0$ on $\mathbb{N}(2\delta)$. Denote $c_i := \max_{\mathbf{x}_t \in \mathcal{D}_i} c(\mathbf{x}_t)$ and $r_i := c_i + \mu - \lambda$ for each $i \in [m]$.

First, given a constant $\sigma > 0$, we define a set

$$\Omega := \left\{ (\mathbf{w}, \mathbf{W}) : \sum_{i=1}^m \alpha_i \left(F_i(\mathbf{w}) + \frac{\lambda}{2} \|\mathbf{w}\|^2 + \frac{\sigma}{2} \|\mathbf{w}_i - \mathbf{w}\|^2 \right) \leq F(\mathbf{w}^0) + \frac{1}{1-\gamma} \right\}, \quad (3.2)$$

where $\gamma := \max_{i \in [m]} \gamma_i$, based on which we further define

$$\delta := \sup_{(\mathbf{w}, \mathbf{W}) \in \Omega} \left\{ \|\mathbf{w}\|, \|\mathbf{w}_1\|, \|\mathbf{w}_2\|, \dots, \|\mathbf{w}_m\| \right\}. \quad (3.3)$$

This indicates that any point $(\mathbf{w}, \mathbf{W}) \in \Omega$ satisfies $\{\mathbf{w}, \mathbf{w}_1, \dots, \mathbf{w}_m\} \subseteq \mathbb{N}(\delta)$. Using this δ , we initialize $\boldsymbol{\sigma}^0 := (\sigma_1^0, \sigma_2^0, \dots, \sigma_m^0)$ by

$$\sigma^0 := \min\{\sigma_1^0, \sigma_2^0, \dots, \sigma_m^0\} \geq 8 \max_{i \in [m]} \left\{ \sigma, \rho_i \eta_i, r_i, \delta^{-2}, \varepsilon_i(2\delta) \right\}. \quad (3.4)$$

It is easy to see that Ω is a bounded set due to F_i being bounded from below. Therefore, δ is bounded and so is $\varepsilon_i(2\delta)$ due to Lemma 3.1. Hence, σ^0 in (3.4) is a well-defined constant, namely, σ^0 can be set as a finite positive number. For notational simplicity, hereafter, we denote

$$\begin{aligned} \Delta \mathbf{w}^\ell &:= \mathbf{w}^\ell - \mathbf{w}^{\ell-1}, & \Delta \mathbf{w}_i^\ell &:= \mathbf{w}_i^\ell - \mathbf{w}_i^{\ell-1} \\ \Delta \boldsymbol{\pi}_i^\ell &:= \boldsymbol{\pi}_i^\ell - \boldsymbol{\pi}_i^{\ell-1}, & \Delta \bar{\mathbf{w}}_i^\ell &:= \mathbf{w}_i^\ell - \mathbf{w}^\ell, \\ \Delta \mathbf{g}_i^\ell &:= \mathbf{g}_i^\ell - \nabla F_i(\mathbf{w}^\ell), & \mathcal{L}^\ell &:= \mathcal{L}(\mathbf{w}^\ell, \mathbf{W}^\ell, \boldsymbol{\Pi}^\ell; \boldsymbol{\sigma}^\ell). \end{aligned} \quad (3.5)$$

Our first result shows the descent property of a merit function associated with \mathcal{L}^ℓ .

Lemma 3.2. Let $\{(\mathbf{w}^\ell, \mathbf{W}^\ell, \boldsymbol{\Pi}^\ell)\}$ be the sequence generated by Algorithm 1 with $\boldsymbol{\sigma}^0$ chosen as (3.4). Then the following statements are valid under Assumption 3.1.

1) For any $\ell \geq 0$, sequence $\{\mathbf{w}^\ell, \mathbf{w}_1^\ell, \dots, \mathbf{w}_m^\ell\} \subseteq \mathbb{N}(\delta)$.

2) For any $\ell \geq 0$,

$$\tilde{\mathcal{L}}^\ell - \tilde{\mathcal{L}}^{\ell+1} \geq \sum_{i=1}^m \alpha_i \left[\frac{\sigma_i^\ell + 2\lambda}{4} \left\| \Delta \mathbf{w}^{\ell+1} \right\|^2 + \frac{\sigma_i^\ell}{4} \left\| \Delta \mathbf{w}_i^{\ell+1} \right\|^2 \right], \quad (3.6)$$

where $\tilde{\mathcal{L}}^\ell$ is defined by

$$\tilde{\mathcal{L}}^\ell := \mathcal{L}^\ell + \sum_{i=1}^m \alpha_i \left[\frac{8}{\sigma_i^\ell} \left\| \rho_i \mathbf{Q}_i^\ell \Delta \bar{\mathbf{w}}_i^\ell \right\|^2 + \frac{\gamma_i^\ell}{16(1-\gamma_i)} \right]. \quad (3.7)$$

The proof of the above lemma is given in Appendix B.3. This lemma is derived from a deterministic perspective. Such a success lies in considering the worst case of bound $\varepsilon_i(2\delta)$ (i.e., taking all possible selections of $\{\mathcal{B}_1^\ell, \dots, \mathcal{B}_m^\ell\}$ into account). Based on the above key lemma, the following theorem shows the sequence convergence of the algorithm.

Theorem 3.1. *Let $\{(\mathbf{w}^\ell, \mathbf{W}^\ell, \mathbf{\Pi}^\ell)\}$ be the sequence generated by Algorithm 1 with $\boldsymbol{\sigma}^0$ chosen as (3.4). Then the following statements are valid under Assumption 3.1.*

1) Sequences $\{\mathcal{L}^\ell\}$ and $\{\tilde{\mathcal{L}}^\ell\}$ converge and for any $i \in [m]$,

$$0 = \lim_{\ell \rightarrow \infty} \|\Delta \mathbf{w}^\ell\| = \lim_{\ell \rightarrow \infty} \|\Delta \mathbf{w}_i^\ell\| = \lim_{\ell \rightarrow \infty} \|\Delta \bar{\mathbf{w}}_i^\ell\| = \lim_{\ell \rightarrow \infty} (\tilde{\mathcal{L}}^\ell - \mathcal{L}^\ell). \quad (3.8)$$

2) Sequence $\{(\mathbf{w}^\ell, \mathbf{W}^\ell, \mathbb{E}\mathbf{\Pi}^\ell)\}$ converges.

The proof of Theorem 3.1 is given in Appendix B.4. To ensure the convergence results, initial value $\boldsymbol{\sigma}^0$ is selected according to (3.4), which involves a hyperparameter δ . If a lower bound \underline{F} of $\min_{\mathbf{w}} \sum_{i=1}^m \alpha_i F_i(\mathbf{w})$ is known, then an upper bound $\bar{\delta}$ for δ can be estimated from (3.2) and (3.3) by substituting $F_i(\mathbf{w})$ with \underline{F} . In practice, particularly in deep learning, many widely used loss functions, such as mean squared error and cross-entropy, yield non-negative values. This observation allows us to set the lower bound as $\underline{F} = 0$. Once $\bar{\delta}$ is estimated, it can be used in (3.4) to select $\boldsymbol{\sigma}^0$, without affecting the convergence guarantees. However, it is worth emphasizing that (3.4) is a sufficient but not necessary condition. Therefore, in practice, it is not essential to enforce this condition strictly when initializing $\boldsymbol{\sigma}^0$ in numerical experiments.

3.2 Complexity analysis

Besides the convergence established above, the algorithm exhibits the following rate of convergence under the same assumption and parameter setup.

Theorem 3.2. *Let $\{(\mathbf{w}^\ell, \mathbf{W}^\ell, \mathbf{\Pi}^\ell)\}$ be the sequence generated by Algorithm 1 with $\boldsymbol{\sigma}^0$ chosen as (3.4). Let \mathbf{w}^∞ be the limit of sequence $\{\mathbf{w}^\ell\}$. Then there is a constant $C_1 > 0$ such that*

$$\max \left\{ \|\mathbf{w}^\ell - \mathbf{w}^\infty\|, \|\mathbf{w}_i^\ell - \mathbf{w}^\infty\|, \|\mathbb{E}\boldsymbol{\pi}_i^\ell + \nabla F_i(\mathbf{w}^\infty)\|, \forall i \in [m] \right\} \leq C_1 \gamma^\ell \quad (3.9)$$

and a constant $C_2 > 0$ such that

$$\max \left\{ F_\lambda(\mathbf{w}^\ell), \mathcal{L}^\ell, \tilde{\mathcal{L}}^\ell \right\} - F_\lambda(\mathbf{w}^\infty) \leq C_2 \gamma^\ell. \quad (3.10)$$

The proof of Theorem 3.2 is given in Appendix B.5. This theorem means that sequence $\{(\mathbf{w}^\ell, \mathbf{W}^\ell, \mathbb{E}\mathbf{\Pi}^\ell)\}$ converges to its limit in a linear rate. To achieve such a result, we only assume Assumption 3.1 without imposing any other commonly used assumptions, such as those presented in Table 1.

4 Precondition Specification

In this section, we explore the preconditioning matrix, namely, matrix \mathbf{Q}_i^ℓ . A simple and computationally efficient choice is to set $\mathbf{Q}_i^\ell = \mathbf{I}$, which enables fast computation of updating $\mathbf{w}_i^{\ell+1}$ via (2.13). However, this choice is too simple to extract useful information about F_i . Therefore, several alternatives can be adopted to set \mathbf{Q}_i^ℓ .

4.1 Second-order Information

Second-order optimization methods, such as Newton-type and trust region methods, are known to enhance numerical performance by leveraging second-order information, the (generalized) Hessian. For instance, if each function F_i is twice continuously differentiable, then one can set

$$\mathbf{Q}_i^{\ell+1} = \nabla^2 F_i(\mathbf{w}^{\ell+1}; \mathcal{B}_i^{\ell+1}), \quad (4.1)$$

where $\nabla^2 F_i(\mathbf{w}^{\ell+1}; \mathcal{B}_i^{\ell+1})$ represents the Hessian of $F_i(\cdot; \mathcal{B}_i^{\ell+1})$ at $\mathbf{w}^{\ell+1}$. With this choice, subproblem (2.8) becomes closely related to second-order methods, and the update takes the form

$$\mathbf{w}_i^{\ell+1} = \mathbf{w}^{\ell+1} - \left(\sigma_i^{\ell+1} \mathbf{I} + \rho_i \nabla^2 F_i(\mathbf{w}^{\ell+1}; \mathcal{B}_i^{\ell+1}) \right)^{-1} \left(\boldsymbol{\pi}_i^\ell + \mathbf{g}_i^{\ell+1} \right).$$

This update corresponds to a Levenberg-Marquardt step [35, 46] or a regularized Newton step [36, 54] when $\sigma_i^{\ell+1} > 0$, and reduces to the classical Newton step if $\sigma_i^{\ell+1} = 0$. While incorporating the Hessian can improve performance in terms of iteration count and solution quality, it often leads to significantly high computational complexity. To mitigate this, some other effective approaches exploit second-moment derived from historical updates to construct the preconditioning matrices.

4.2 Second Moment

We note that the second moment to determine an adaptive learning rate enables the improvements of the learning performance of several popular algorithms, such as RMSProp [68] and Adam [31]. Motivated by this, we specify preconditioning matrix by using the second moment as follows,

$$\mathbf{Q}_i^{\ell+1} = \text{Diag} \left(\sqrt{\mathbf{m}_i^{\ell+1}} \right), \quad (4.2)$$

where $\text{Diag}(\mathbf{m})$ is the diagonal matrix with the diagonal entries formed by \mathbf{m} and $\mathbf{m}_i^{\ell+1}$ can be chosen flexibly as long as it satisfies that $\|\mathbf{m}_i^{\ell+1}\|_\infty \leq \eta_i^2$. Here, $\|\mathbf{m}\|_\infty$ is the infinity norm of \mathbf{m} . We can set $\mathbf{m}_i^{\ell+1}$ as follows

$$\mathbf{m}_i^{\ell+1} = \min \left\{ \tilde{\mathbf{m}}_i^{\ell+1}, \eta_i^2 \mathbf{1} \right\}, \quad (4.3)$$

where $\tilde{\mathbf{m}}_i^{\ell+1}$ can be updated by

$$\begin{aligned} \text{Scheme I:} \quad & \tilde{\mathbf{m}}_i^{\ell+1} = \tilde{\mathbf{m}}_i^\ell + \left(\boldsymbol{\pi}_i^\ell + \mathbf{g}_i^{\ell+1} \right) \odot \left(\boldsymbol{\pi}_i^\ell + \mathbf{g}_i^{\ell+1} \right), \\ \text{Scheme II:} \quad & \tilde{\mathbf{m}}_i^{\ell+1} = \beta_i \tilde{\mathbf{m}}_i^\ell + (1 - \beta_i) \left(\boldsymbol{\pi}_i^\ell + \mathbf{g}_i^{\ell+1} \right) \odot \left(\boldsymbol{\pi}_i^\ell + \mathbf{g}_i^{\ell+1} \right), \\ \text{Scheme III:} \quad & \mathbf{n}_i^{\ell+1} = \beta_i \mathbf{n}_i^\ell + (1 - \beta_i) \left(\boldsymbol{\pi}_i^\ell + \mathbf{g}_i^{\ell+1} \right) \odot \left(\boldsymbol{\pi}_i^\ell + \mathbf{g}_i^{\ell+1} \right), \\ & \tilde{\mathbf{m}}_i^{\ell+1} = \mathbf{n}_i^{\ell+1} / (1 - \beta_i^{\ell+1}), \end{aligned} \quad (4.4)$$

Algorithm 2: Second moment-based Inexact Stochastic ADMM (SISA).

Divide \mathcal{D} into m disjoint batches $\{\mathcal{D}_1, \mathcal{D}_2, \dots, \mathcal{D}_m\}$ and calculate α_i by (2.1).

Initialize $\mathbf{w}^0 = \mathbf{w}_i^0 = \boldsymbol{\pi}_i^0 = 0$, $\gamma_i \in [3/4, 1)$, and $(\sigma_i^0, \eta_i, \rho_i) > 0$ for each $i \in [m]$.

for $\ell = 0, 1, 2, \dots$ **do**

for $i = 1, 2, \dots, m$ **do**

$$\mathbf{w}^{\ell+1} = \frac{\sum_{i=1}^m \alpha_i (\sigma_i^\ell \mathbf{w}_i^\ell + \boldsymbol{\pi}_i^\ell)}{\sum_{i=1}^m \alpha_i \sigma_i^\ell + \lambda}.$$

 Randomly draw a mini-batch $\mathcal{B}_i^{\ell+1} \in \mathcal{D}_i$ and calculate $\mathbf{g}_i^{\ell+1} = \nabla F_i(\mathbf{w}^{\ell+1}; \mathcal{B}_i^{\ell+1})$.

 Choose $\mathbf{m}_i^{\ell+1}$ to satisfy $\|\mathbf{m}_i^{\ell+1}\|_\infty \leq \eta_i^2$.

$$\sigma_i^{\ell+1} = \sigma_i^\ell / \gamma_i.$$

$$\mathbf{w}_i^{\ell+1} = \mathbf{w}^{\ell+1} - \frac{\boldsymbol{\pi}_i^\ell + \mathbf{g}_i^{\ell+1}}{\sigma_i^{\ell+1} + \rho_i \sqrt{\mathbf{m}_i^{\ell+1}}}. \quad (4.5)$$

$$\boldsymbol{\pi}_i^{\ell+1} = \boldsymbol{\pi}_i^\ell + \sigma_i^{\ell+1} (\mathbf{w}_i^{\ell+1} - \mathbf{w}^{\ell+1}).$$

end

end

where $\tilde{\mathbf{m}}_i^0$ and \mathbf{n}_i^0 are given, $\beta_i \in (0, 1)$, and β_i^ℓ stands for power ℓ of β_i . These three schemes resemble the ones used by AdaGrad [16], RMSProp [68], and Adam [31], respectively. Employing (4.2) into Algorithm 1 gives rise to Algorithm 2. We term it SISA, an abbreviation for the second moment-based inexact SADMM. Compared to PISA in Algorithm 1, SISA admits three advantages.

- i) It is capable of incorporating various schemes of the second moment, which may enhance the numerical performance of SISA significantly.
- ii) One can easily check that $\eta_i \mathbf{I} \succeq \mathbf{Q}_i^{\ell+1} \succeq 0$ for each batch $i \in [m]$ and all $\ell \geq 1$. Therefore, (4.2) enables us to preserve the convergence property as follows.

Theorem 4.1. *Let $\{(\mathbf{w}^\ell, \mathbf{W}^\ell, \boldsymbol{\Pi}^\ell)\}$ be the sequence generated by Algorithm 2 with $\boldsymbol{\sigma}^0$ chosen as (3.4). Then under Assumption 3.1, all statements in Theorems 3.1 and 3.2 are valid.*

- iii) Such a choice of $\mathbf{Q}_i^{\ell+1}$ enables the fast computation compared to update $\mathbf{w}_i^{\ell+1}$ by (2.8). In fact, since operation \mathbf{u}/\mathbf{v} denotes element-wise division, the complexity of computing (4.5) is $O(p)$, where p is the dimension of $\mathbf{w}_i^{\ell+1}$, whereas the complexity of computing (2.13) is $O(p^3)$.

4.3 Orthogonalized Momentum by Newton-Schulz Iterations

Recently, the authors of [29] proposed an algorithm called Muon, which orthogonalizes momentum using Newton-Schulz iterations. This approach has shown promising results in fine-tuning LLMs,

Algorithm 3: Newton-Schulz-based Inexact Stochastic ADMM (NSISA).

Divide \mathcal{D} into m disjoint batches $\{\mathcal{D}_1, \mathcal{D}_2, \dots, \mathcal{D}_m\}$ and calculate α_i by (2.1).

Initialize $\mathbf{w}^0 = \mathbf{w}_i^0 = \boldsymbol{\pi}_i^0 = \mathbf{b}_i^0 = 0$, $\gamma_i \in [3/4, 1)$, $\epsilon_i \in (0, 1)$, and $(\sigma_i^0, \rho_i, \mu_i) > 0$ for each $i \in [m]$.

for $\ell = 0, 1, 2, \dots$ **do**

$$\mathbf{w}^{\ell+1} = \frac{\sum_{i=1}^m \alpha_i (\sigma_i^\ell \mathbf{w}_i^\ell + \boldsymbol{\pi}_i^\ell)}{\sum_{i=1}^m \alpha_i \sigma_i^\ell + \lambda}.$$

for $i = 1, 2, \dots, m$ **do**

Randomly draw a mini-batch $\mathcal{B}_i^{\ell+1} \in \mathcal{D}_i$ and calculate $\mathbf{g}_i^{\ell+1} = \nabla F_i(\mathbf{w}^{\ell+1}; \mathcal{B}_i^{\ell+1})$.

$$\mathbf{b}_i^{\ell+1} = \mu_i \mathbf{b}_i^\ell + \mathbf{g}_i^{\ell+1}.$$

$$\mathbf{o}_i^{\ell+1} = \text{NewtonSchulz}(\mathbf{b}_i^{\ell+1}).$$

$$\sigma_i^{\ell+1} = \sigma_i^\ell / \gamma_i.$$

$$\mathbf{w}_i^{\ell+1} = \mathbf{w}^{\ell+1} - \frac{\boldsymbol{\pi}_i^\ell + \mathbf{o}_i^{\ell+1} + \epsilon_i^{\ell+1} \mathbf{v}_i^{\ell+1}}{\sigma_i^{\ell+1} + \rho_i \sqrt{\mathbf{m}_i^{\ell+1}}}. \quad (4.6)$$

$$\boldsymbol{\pi}_i^{\ell+1} = \boldsymbol{\pi}_i^\ell + \sigma_i^{\ell+1} (\mathbf{w}_i^{\ell+1} - \mathbf{w}^{\ell+1}).$$

end

end

outperforming many established optimizers. The underlying philosophy of Muon can also inform the design of the preconditioning matrix. Specifically, we consider the two-dimensional case, namely, the trainable variable \mathbf{w} is a matrix. Then subproblem (2.8) in a vector form turns to

$$\text{vec}(\mathbf{w}_i^{\ell+1}) = \text{vec}(\mathbf{w}^{\ell+1}) - \left(\sigma_i^{\ell+1} \mathbf{I} + \rho_i \mathbf{Q}_i^{\ell+1} \right)^{-1} \left(\text{vec}(\boldsymbol{\pi}_i^\ell) + \text{vec}(\mathbf{g}_i^{\ell+1}) \right), \quad (4.7)$$

where $\text{vec}(\mathbf{w})$ denotes the column-wise vectorization of matrix \mathbf{w} . Now, initialize \mathbf{b}_i^0 for all $i \in [m]$ and $\mu > 0$, update momentum by $\mathbf{b}_i^{\ell+1} = \mu \mathbf{b}_i^\ell + \mathbf{g}_i^{\ell+1}$. Let $\mathbf{b}_i^{\ell+1} = \mathbf{U}_i^{\ell+1} \boldsymbol{\Lambda}_i^{\ell+1} (\mathbf{V}_i^{\ell+1})^\top$ be the singular value decomposition of $\mathbf{b}_i^{\ell+1}$, where $\boldsymbol{\Lambda}_i^{\ell+1}$ is an diagonal matrix and $\mathbf{U}_i^{\ell+1}$ and $\mathbf{V}_i^{\ell+1}$ are two orthogonal matrices. Compute $\mathbf{o}_i^{\ell+1} = \mathbf{U}_i^{\ell+1} (\mathbf{V}_i^{\ell+1})^\top$ and $\mathbf{p}_i^{\ell+1}$ by

$$\mathbf{p}_i^\ell = \frac{\left(\sigma_i^{\ell+1} + \rho_i \sqrt{\mathbf{m}_i^{\ell+1}} \right) \odot \left(\boldsymbol{\pi}_i^\ell + \mathbf{g}_i^{\ell+1} \right)}{\rho_i \left(\boldsymbol{\pi}_i^\ell + \mathbf{o}_i^{\ell+1} + \epsilon_i^{\ell+1} \mathbf{v}_i^{\ell+1} \right)} - \frac{\sigma_i^{\ell+1}}{\rho_i},$$

where $\mathbf{m}_i^{\ell+1}$ can be the second moment (e.g., $\mathbf{m}_i^{\ell+1} = (\boldsymbol{\pi}_i^\ell + \mathbf{o}_i^{\ell+1}) \odot (\boldsymbol{\pi}_i^\ell + \mathbf{o}_i^{\ell+1})$ is used in the numerical experiment), $\epsilon_i \in (0, 1)$ (here, ϵ_i^ℓ stands for power ℓ of ϵ_i), and $\mathbf{v}_i^{\ell+1}$ is a matrix with (k, j) th element computed by $(\mathbf{v}_i^{\ell+1})_{kj} = 1$ if $(\boldsymbol{\pi}_i^\ell + \mathbf{o}_i^{\ell+1})_{kj} = 0$ and $(\mathbf{v}_i^{\ell+1})_{kj} = 0$ otherwise. Then we set the preconditioning matrix by

$$\mathbf{Q}_i^{\ell+1} = \text{Diag} \left(\text{vec}(\mathbf{p}_i^{\ell+1}) \right).$$

Substituting above choice into (4.7) derives (4.6). The idea of using (4.6) is inspired by [29], where Newton–Schulz orthogonalization [32, 5] is employed to efficiently approximate $\mathbf{o}_i^{\ell+1}$. Incorporating these steps into Algorithm 1 leads to Algorithm 3, which we refer to as NSISA, short for Newton–Schulz-based Inexact SADMM. The implementation of `NewtonSchulz(b)` is provided in [29]. Below is the convergence result of NSISA.

Theorem 4.2. *Let $\{(\mathbf{w}^\ell, \mathbf{W}^\ell, \mathbf{\Pi}^\ell)\}$ be the sequence generated by Algorithm 3 with $\boldsymbol{\sigma}^0$ chosen as (3.4). If Assumption 3.1 holds and $(\mathbf{p}_i^\ell)_{kj} \in (0, \eta_i)$ for any (k, j) and $\ell \geq 0$, all statements in Theorems 3.1 and 3.2 are valid.*

5 Numerical Experiments

This section evaluates the performance of SISA and NSISA in comparison with various established optimizers to process several deep models: VMs, LLMs, RLMs, GANs, and RNNs. All LLM-targeted experiments are conducted on four NVIDIA H100-80GB GPUs, while the remaining experiments are run on a single such GPU. The source codes are available at <https://github.com/Tracy-Wang7/PISA>. Due to space limitations, details on hyperparameter setup, effects of key hyperparameters, and experiments on RLMs and RNNs are provided in Appendix A.

5.1 Data Heterogeneity

To evaluate the effectiveness of the proposed algorithms in addressing the challenge of data heterogeneity, we design some experiments within a centralized federated learning (CFL) framework. In this setting, m clients collaboratively learn a shared parameter under a central server, with each

Table 2: Testing accuracy under data heterogeneity with skewed label distributions.

Dataset	Partition	Fedavg	Fedprox	Fednova	Scaffold	SISA
MNIST	1-Label	53.19 \pm 0.21	54.33 \pm 0.67	49.00 \pm 0.42	47.04 \pm 0.02	94.97 \pm 0.01
	2-Label	90.70 \pm 0.02	90.75 \pm 0.03	90.40 \pm 0.05	87.43 \pm 0.08	96.14 \pm 0.00
	3-Label	95.11 \pm 0.01	94.73 \pm 0.02	94.37 \pm 0.01	93.19 \pm 0.03	96.21 \pm 0.01
CIFAR10	1-Label	10.02 \pm 0.00	10.00 \pm 0.00	10.31 \pm 0.03	11.41 \pm 0.03	30.16 \pm 0.00
	2-Label	13.76 \pm 0.00	13.77 \pm 0.00	18.02 \pm 0.02	12.73 \pm 0.00	30.53 \pm 0.00
	3-Label	20.06 \pm 0.01	20.03 \pm 0.01	21.20 \pm 0.01	17.00 \pm 0.00	30.96 \pm 0.00
FMNIST	1-Label	48.81 \pm 0.34	47.14 \pm 0.32	49.08 \pm 0.34	43.93 \pm 0.20	72.85 \pm 0.02
	2-Label	69.33 \pm 0.01	69.29 \pm 0.02	69.10 \pm 0.04	65.99 \pm 0.06	70.24 \pm 0.05
	3-Label	70.48 \pm 0.02	69.96 \pm 0.08	69.70 \pm 0.08	63.64 \pm 0.15	72.46 \pm 0.01
Adult	1-Label	76.38* \pm 0.00	78.30* \pm 0.03	85.15* \pm 0.08	80.00* \pm 0.02	82.21 \pm 0.00

* indicates mini-batch training in each local client. Higher values indicate better performance.

client i holding a local dataset \mathcal{D}_i . Note that our three algorithms are well-suited for CFL tasks. As shown in Algorithm 2, clients update their local parameters $(\mathbf{w}_i^{\ell+1}, \boldsymbol{\pi}_i^{\ell+1})$ in parallel, and the server aggregates them to compute global parameter $\mathbf{w}^{\ell+2}$.

In the experiment, we focus on heterogeneous datasets $\mathcal{D}_1, \mathcal{D}_2, \dots, \mathcal{D}_m$. The heterogeneity may arise from label distribution skew, feature distribution skew, or quantity skew [37]. Empirical evidence has shown that the label distribution skew presents a significantly greater challenge to current FL methods compared to the other two types. Therefore, we adopt this skew as the primary setting for evaluating data heterogeneity in our experiments.

To reflect the fact that most benchmark datasets contain 10 image classes, we set $m = 10$. Four datasets: MNIST, CIFAR10, FMNIST, and Adult are used for the experiment. As shown in Table 2, the configuration ‘ s -Label’ indicates that each client holds data containing s distinct label classes, where $s = 1, 2, 3$. For example, in the ‘2-Label’ setting, \mathcal{D}_1 may include two labels 1 and 2, while \mathcal{D}_2 contains two labels 2 and 3. To ensure better performance, we employed a mini-batch training strategy with multiple local updates before each aggregation step for the five baseline algorithms. In contrast, SISA keeps using one local update per aggregation step and still achieves competitive testing accuracy with far fewer local updates. Notably, on the MNIST dataset under the 1-Label skew setting, the best accuracy achieved by other algorithms is 54.33%, whereas SISA reaches 94.97%, demonstrating a significant improvement.

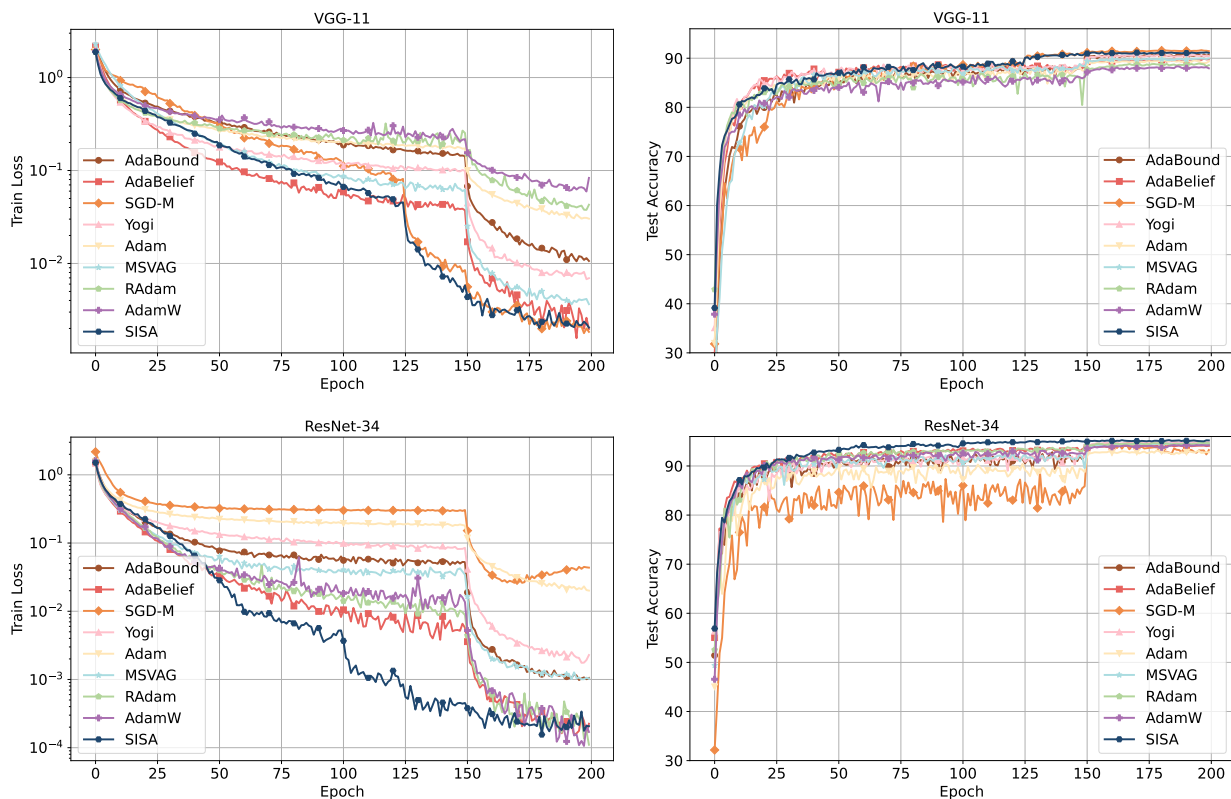


Figure 1: Training loss and testing accuracy over epochs for VMs on Cifar-10.

5.2 Classification by VMs

We perform classification tasks on two well-known datasets: ImageNet [34] and CIFAR-10 [33], and evaluate performance based on convergence speed and testing accuracy. Convergence results are presented in Appendix A.3. We now focus on testing accuracy, following the experimental setup and hyperparameter configurations from [97]. In this experiment, a small batch size (e.g., $|\mathcal{D}_i| = 128$ for every $i \in [m]$) is used during training. As SISA updates its hyperparameters frequently, it uses a different learning rate scheduler from that in [97]. For fair comparison, each baseline optimizer is tested with both its default scheduler and the one employed by SISA, and the best result is reported. On CIFAR-10, we train three models: VGG-11 [64], ResNet-34 [24], and DenseNet-121 [28]. As shown in Table 3, SISA achieves the highest testing accuracy on ResNet-34 and DenseNet-121, and performs slightly worse than SGD-M on VGG-11. Additionally, Figure 1 illustrates the training loss and testing accuracy over training epochs for VGG-11 and ResNet-34, demonstrating the fast convergence and high accuracy of SISA. For ImageNet, we train a ResNet-18 model and report the testing accuracy in Table 3. SISA outperforms most adaptive methods but is slightly behind SGD-M and AdaBelief.

Table 3: Top-1 Acc. (%) obtained by different algorithms.

Algs.	SISA	SGD-M	AdaBd	Adam	Radam	MSVAG	AdamW	AdaBf	Yogi	LAMB	Nadam
Refs.	[60]	[60]	[44]	[31]	[41]	[4]	[43]	[97]	[86]	[84]	[14]
ResNet-34	95.04	94.65*	94.33*	94.69*	94.20	94.44*	94.28*	94.11*	94.52*	94.01*	–
VGG-11	91.25	91.51	90.62*	88.40*	89.30*	90.24*	89.39*	90.07	90.67*	87.48	–
DenseNet-121	95.77	95.47	94.58*	93.35*	94.91*	94.81*	94.55*	94.78	95.15	94.53	–
ResNet-18	70.03	70.23*	68.13*	63.79*	67.62*	65.99*	67.93*	70.08*	–	68.46*	68.82*

* and \star are reported in [78] and [97], and the remaining are derived by our implementation. Higher values indicate better performance. ‘–’ means no results were reported. AdaBd and AdaBf stand for AdaBound and AdaBelief, respectively.

5.3 Training LLMs

In this subsection, we apply SISA and NSISA to train several GPT2 models [57] and compare it with advanced optimizers like AdamW, Muon, Shampoo, SOAP, and Adam-mini that have been proven to be effective in training LLM. The comparison between SISA and AdamW is provided in Appendix A.4. We now compare NSISA with the other four optimizers, with the aim of tuning three GPT2 models: GPT2-Nano (125M), GPT2-Medium (330M), and GPT2-XL (1.5B). The first model follows the setup described [29], while the latter two follow the configuration from [93]. We use the FineWeb dataset, a large collection of high-quality web text, to fine-tune GPT2 models, enabling them to generate more coherent and contextually relevant web-style content. The hyperparameters of NSISA remain consistent across the experiments for the three GPT2 models.

The comparison of different algorithms in terms of the memory overhead is given in Appendix

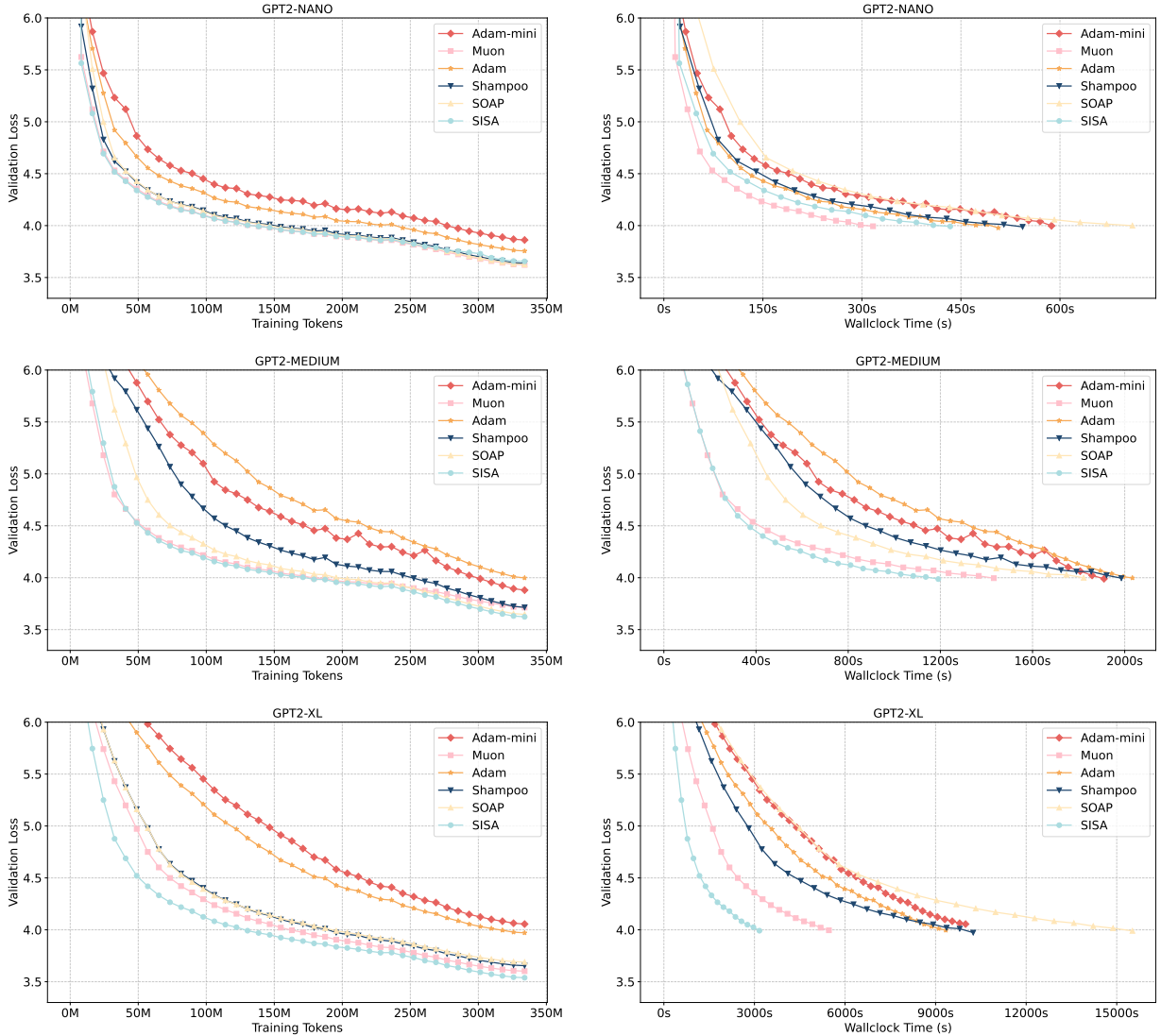


Figure 2: Validation loss over tokens and wall-clock time (in seconds) for three GPT2 models.

A.4. The experimental results are presented in Figure 2. We evaluate each optimizer’s training performance from two perspectives: the number of training tokens consumed and the wall-clock time required. To reduce wall-clock time, we implemented NSISA using parallel computation. From Figure 2, as the number of GPT2 parameters increases from Nano to Medium to XL, the validation loss gap between NSISA and other baseline optimizers widens. In particular, for GPT2-XL, the last figure demonstrated evident advantage of NSISA in terms of the wall-clock time.

5.4 Generation tasks by GANs

GANs involve alternating updates between the generator and discriminator in a minimax game, making training notoriously unstable [20]. To assess optimizer stability, we compare SISA with adaptive methods such as Adam, RMSProp, and AdaBelief, which are commonly recommended to enhance both stability and efficiency in training GANs [63, 97]. We use two popular architectures, the Wasserstein GAN (WGAN [3]) and WGAN with gradient penalty (WGAN-GP [63]), with a

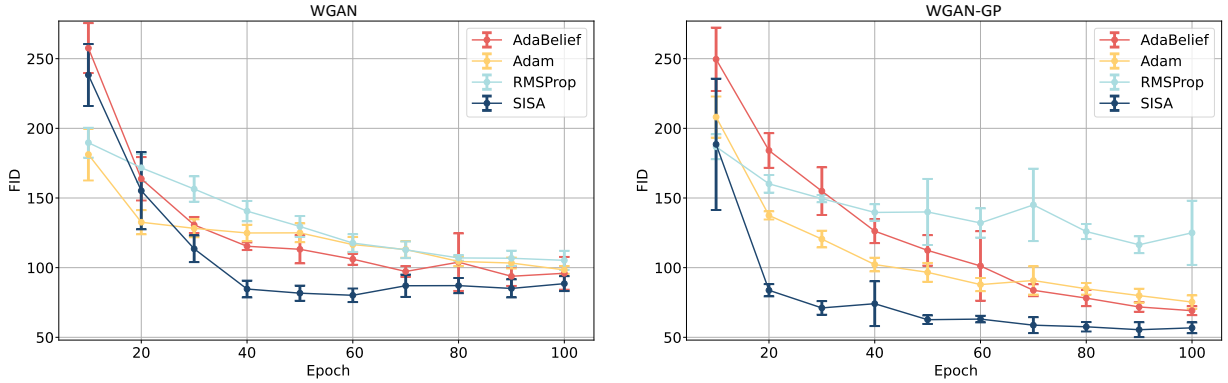


Figure 3: Training FID over epochs for GANs on Cifar-10.

Table 4: Testing FID after training GANs on Cifar-10.

	SISA	Adam	RMSProp	AdaBelief
WGAN	85.07 ± 5.49	95.06 ± 2.97	102.39 ± 7.05	92.37 ± 11.13
WGAN_GP	53.34 ± 3.87	71.38 ± 5.04	121.62 ± 22.79	65.71 ± 3.36

small model and vanilla CNN generator on the CIFAR-10 dataset.

To evaluate performance, we compute the Fréchet Inception Distance (FID) [25] every 10 training epochs, measuring the distance between 6,400 generated images and 60,000 real images. The FID score is a widely used metric for generative models, assessing both image quality and diversity. The lower FID values indicate better generated images. We follow the experimental setup from [97] and run each optimizer five times independently. The corresponding mean and standard deviation of training FID over epochs are presented in Figure 3. Clearly, SISA achieves the fastest convergence and the lowest FID. After training, 64,000 fake images are produced to compute the testing FID in Table 4. Once again, SISA outperforms the other three optimizers, demonstrating its superior stability and effectiveness in training GANs.

6 Conclusion

This paper introduces an ADMM-based algorithm that leverages stochastic gradients and solves sub-problems inexactly, significantly accelerating computation. The preconditioning framework allows it to incorporate popular second-moment schemes, enhancing training performance. Theoretical guarantees, based solely on the Lipschitz continuity of the gradients, make the algorithm suitable for heterogeneous datasets, effectively addressing an open problem in stochastic optimization for distributed learning. The algorithm demonstrates superior generalization across a wide range of architectures, datasets, and tasks, outperforming well-known deep learning optimizers.

References

- [1] A. Agarwal, M. J. Wainwright, and J. C. Duchi. Distributed dual averaging in networks. *Adv. Neural Inform. Process. Syst.*, 23, 2010.
- [2] N. Agarwal, B. Bullins, X. Chen, E. Hazan, K. Singh, C. Zhang, and Y. Zhang. Efficient full-matrix adaptive regularization. In *ICML*, pages 102–110, 2019.
- [3] M. Arjovsky, S. Chintala, and L. Bottou. Wasserstein generative adversarial networks. In *ICML*, pages 214–223. PMLR, 2017.
- [4] L. Balles and P. Hennig. Dissecting adam: The sign, magnitude and variance of stochastic gradients. In *ICML*, pages 404–413, 2018.
- [5] Å. Björck and C. Bowie. An iterative algorithm for computing the best estimate of an orthogonal matrix. *SIAM J. Numer. Anal.*, 8(2):358–364, 1971.
- [6] L. Bottou. Large-scale machine learning with stochastic gradient descent. In *COMPSTAT*, pages 177–186. Springer, 2010.
- [7] L. Bottou, F. E. Curtis, and J. Nocedal. Optimization methods for large-scale machine learning. *SIAM Rev.*, 60(2):223–311, 2018.
- [8] S. Boyd, N. Parikh, E. Chu, B. Peleato, J. Eckstein, et al. Distributed optimization and statistical learning via the alternating direction method of multipliers. *Found. Trends Mach. Learn.*, 3(1):1–122, 2011.
- [9] J. Chen, D. Zhou, Y. Tang, Z. Yang, Y. Cao, and Q. Gu. Closing the generalization gap of adaptive gradient methods in training deep neural networks. In *IJCAI*, pages 3267–3275, 2018.
- [10] X. Chen, C. Liang, D. Huang, E. Real, K. Wang, Y. Liu, H. Pham, X. Dong, T. Luong, C.-J. Hsieh, et al. Symbolic discovery of optimization algorithms. *arXiv preprint arXiv:2302.06675*, 2023.
- [11] K. L. Chung. On a stochastic approximation method. *Ann. Math. Stat.*, pages 463–483, 1954.
- [12] J. Ding, S. M. Errapotu, H. Zhang, Y. Gong, M. Pan, and Z. Han. Stochastic ADMM based distributed machine learning with differential privacy. In *SecureComm*, pages 257–277, 2019.
- [13] A. Dosovitskiy, L. Beyer, A. Kolesnikov, D. Weissenborn, X. Zhai, T. Unterthiner, M. Dehghani, M. Minderer, G. Heigold, S. Gelly, J. Uszkoreit, and N. Houlsby. An image is worth 16x16 words: Transformers for image recognition at scale. In *ICLR*, 2021.
- [14] T. Dozat. Incorporating nesterov momentum into adam. In *ICLR*, 2016.
- [15] Y. Duan, X. Chen, R. Houthoofd, J. Schulman, and P. Abbeel. Benchmarking deep reinforcement learning for continuous control. In *ICML*, pages 1329–1338. PMLR, 2016.

- [16] J. Duchi, E. Hazan, and Y. Singer. Adaptive subgradient methods for online learning and stochastic optimization. *J. Mach. Learn. Res.*, 12(7):2121–2159, 2011.
- [17] J. C. Duchi, A. Agarwal, and M. J. Wainwright. Dual averaging for distributed optimization: Convergence analysis and network scaling. *IEEE Trans. Automat. Contr.*, 57(3):592–606, 2011.
- [18] Z. Ebrahimi, G. Batista, and M. Deghat. AA-DLADMM: An accelerated ADMM-based framework for training deep neural networks. *arXiv preprint arXiv:2401.03619*, 2024.
- [19] D. Gabay and B. Mercier. A dual algorithm for the solution of nonlinear variational problems via finite element approximation. *Comput. Math. Appl.*, 2(1):17–40, 1976.
- [20] I. Goodfellow, J. Pouget-Abadie, M. Mirza, B. Xu, D. Warde-Farley, S. Ozair, A. Courville, and Y. Bengio. Generative adversarial nets. *NeurIPS*, 27, 2014.
- [21] A. Graves and A. Graves. *Long short-term memory*. Springer, 2012.
- [22] V. Gupta, T. Koren, and Y. Singer. Shampoo: Preconditioned stochastic tensor optimization. In *ICML*, pages 1842–1850, 2018.
- [23] K. He, X. Zhang, S. Ren, and J. Sun. Deep residual learning for image recognition. In *CVPR*, pages 770–778. IEEE, 2016.
- [24] K. He, X. Zhang, S. Ren, and J. Sun. Identity mappings in deep residual networks. In *ECCV*, pages 630–645. Springer, 2016.
- [25] M. Heusel, H. Ramsauer, T. Unterthiner, B. Nessler, and S. Hochreiter. Gans trained by a two time-scale update rule converge to a local nash equilibrium. *NeurIPS*, 30, 2017.
- [26] S. Hosseini, A. Chapman, and M. Mesbahi. Online distributed optimization via dual averaging. In *CDC*, pages 1484–1489. IEEE, 2013.
- [27] F. Huang, S. Chen, and H. Huang. Faster stochastic alternating direction method of multipliers for nonconvex optimization. In *ICML*, pages 2839–2848, 2019.
- [28] G. Huang, Z. Liu, L. Van Der Maaten, and K. Q. Weinberger. Densely connected convolutional networks. In *CVPR*, pages 4700–4708. IEEE, 2017.
- [29] K. Jordan, Y. Jin, V. Boza, J. You, F. Cesista, L. Newhouse, and J. Bernstein. Muon: An optimizer for hidden layers in neural networks, 2024.
- [30] P. Kairouz, H. B. McMahan, B. Avent, A. Bellet, M. Bennis, A. N. Bhagoji, K. Bonawitz, Z. Charles, G. Cormode, R. Cummings, et al. Advances and open problems in federated learning. *Found. Trends Mach. Learn.*, 14(1–2):1–210, 2021.
- [31] D. P. Kingma. Adam: A method for stochastic optimization. In *ICLR*, 2015.
- [32] Z. Kovarik. Some iterative methods for improving orthonormality. *SIAM J. Numer. Anal.*, 7(3):386–389, 1970.

- [33] A. Krizhevsky, V. Nair, and G. Hinton. Cifar-10 (canadian institute for advanced research). URL <http://www.cs.toronto.edu/kriz/cifar.html>, 5(4):1, 2010.
- [34] A. Krizhevsky, I. Sutskever, and G. E. Hinton. Imagenet classification with deep convolutional neural networks. *NeurIPS*, 25, 2012.
- [35] K. Levenberg. A method for the solution of certain non-linear problems in least squares. *Q. Appl. Math.*, 2(2):164–168, 1944.
- [36] D.-H. Li, M. Fukushima, L. Qi, and N. Yamashita. Regularized newton methods for convex minimization problems with singular solutions. *Comput. Optim. Appl.*, 28:131–147, 2004.
- [37] Q. Li, Y. Diao, Q. Chen, and B. He. Federated learning on non-iid data silos: An experimental study. In *ICDE*, pages 965–978. IEEE, 2022.
- [38] T. Li, A. K. Sahu, M. Zaheer, M. Sanjabi, A. Talwalkar, and V. Smith. Federated optimization in heterogeneous networks. *MLSys*, 2:429–450, 2020.
- [39] X. Li, K. Huang, W. Yang, S. Wang, and Z. Zhang. On the convergence of FedAvg on non-iid data. In *ICLR*, 2020.
- [40] X.-L. Li. Preconditioned stochastic gradient descent. *IEEE Trans. Neural Netw. Learn. Syst.*, 29(5):1454–1466, 2017.
- [41] L. Liu, H. Jiang, P. He, W. Chen, X. Liu, J. Gao, and J. Han. On the variance of the adaptive learning rate and beyond. In *ICLR*, 2020.
- [42] Y. Liu, F. Shang, and J. Cheng. Accelerated variance reduced stochastic ADMM. In *AAAI*, volume 31, 2017.
- [43] I. Loshchilov. Decoupled weight decay regularization. In *ICLR*, 2018.
- [44] L. Luo, Y. Xiong, Y. Liu, and X. Sun. Adaptive gradient methods with dynamic bound of learning rate. In *ICLR*, 2019.
- [45] M. Marcus, B. Santorini, and M. A. Marcinkiewicz. Building a large annotated corpus of english: The penn treebank. *Comput. Linguist.*, 19(2):313–330, 1993.
- [46] D. W. Marquardt. An algorithm for least-squares estimation of nonlinear parameters. *J. Soc. Ind. Appl. Math*, 11(2):431–441, 1963.
- [47] B. McMahan, E. Moore, D. Ramage, S. Hampson, and B. A. y Arcas. Communication-efficient learning of deep networks from decentralized data. In *AISTATS*, pages 1273–1282, 2017.
- [48] M. C. Mukkamala and M. Hein. Variants of RMSProp and Adagrad with logarithmic regret bounds. In *ICML*, pages 2545–2553, 2017.
- [49] Y. Nesterov. A method for solving the convex programming problem with convergence rate $o(1/k^2)$. In *Dokl akad nauk Sssr*, volume 269, page 543, 1983.

- [50] Y. Nesterov. On an approach to the construction of optimal methods of minimization of smooth convex functions. *Ekonomika i Matematicheskie Metody*, 24(3):509–517, 1988.
- [51] R. Novak, Y. Bahri, D. A. Abolafia, J. Pennington, and J. Sohl-Dickstein. Sensitivity and generalization in neural networks: An empirical study. *arXiv preprint arXiv:1802.08760*, 2018.
- [52] OpenAI, J. Achiam, S. Adler, S. Agarwal, L. Ahmad, I. Akkaya, F. L. Aleman, D. Almeida, J. Altschmidt, and et al. GPT-4 technical report. *arXiv:2303.08774*, 2024.
- [53] H. Ouyang, N. He, L. Tran, and A. Gray. Stochastic alternating direction method of multipliers. In *ICML*, pages 80–88, 2013.
- [54] R. A. Polyak. Regularized newton method for unconstrained convex optimization. *Math. Program.*, 120:125–145, 2009.
- [55] S. Pu, W. Shi, J. Xu, and A. Nedić. Push–pull gradient methods for distributed optimization in networks. *IEEE Trans. Autom. Control.*, 66(1):1–16, 2020.
- [56] N. Qian. On the momentum term in gradient descent learning algorithms. *Neural Netw.*, 12(1):145–151, 1999.
- [57] A. Radford, J. Wu, R. Child, D. Luan, D. Amodei, I. Sutskever, et al. Language models are unsupervised multitask learners. *OpenAI Blog*, 1(8):9, 2019.
- [58] S. J. Reddi, Z. Charles, M. Zaheer, Z. Garrett, K. Rush, J. Konečný, S. Kumar, and H. B. McMahan. Adaptive federated optimization. In *ICLR*, 2021.
- [59] S. J. Reddi, S. Kale, and S. Kumar. On the convergence of Adam and beyond. In *ICLR*, 2018.
- [60] H. Robbins and S. Monro. A stochastic approximation method. *Ann. Math. Stat.*, pages 400–407, 1951.
- [61] R. T. Rockafellar and R. J.-B. Wets. *Variational analysis*, volume 317. Springer Science & Business Media, 2009.
- [62] S. Ruder. An overview of gradient descent optimization algorithms. *arXiv:1609.04747*, 2016.
- [63] T. Salimans, I. Goodfellow, W. Zaremba, V. Cheung, A. Radford, and X. Chen. Improved techniques for training gans. *NeurIPS*, 29, 2016.
- [64] K. Simonyan and A. Zisserman. Very deep convolutional networks for large-scale image recognition. *arXiv preprint arXiv:1409.1556*, 2014.
- [65] S. U. Stich. Local SGD converges fast and communicates little. In *ICLR*, 2019.
- [66] G. Taylor, R. Burmeister, Z. Xu, B. Singh, A. Patel, and T. Goldstein. Training neural networks without gradients: A scalable ADMM approach. In *ICML*, pages 2722–2731, 2016.
- [67] G. Team, T. Mesnard, C. Hardin, R. Dadashi, S. Bhupatiraju, S. Pathak, L. Sifre, and et al. Gemma: Open models based on gemini research and technology. *arXiv:2403.08295*, 2024.

- [68] T. Tieleman. Lecture 6.5-rmsprop: Divide the gradient by a running average of its recent magnitude. *COURSERA: Neural networks for machine learning*, 4(2):26, 2012.
- [69] E. Todorov, T. Erez, and Y. Tassa. Mujoco: A physics engine for model-based control. In *IEEE/RSJ IROS*, pages 5026–5033. IEEE, 2012.
- [70] H. Touvron, L. Martin, K. Stone, P. Albert, A. Almahairi, Y. Babaei, N. Bashlykov, S. Batra, and et al. Llama 2: Open foundation and fine-tuned chat models. *arXiv:2307.09288*, 2023.
- [71] T. Tran. Fine-tuning large language model with hugging face & PyTorch, 2023. Accessed: 2024-01-31.
- [72] K. I. Tsianos, S. Lawlor, and M. G. Rabbat. Push-sum distributed dual averaging for convex optimization. In *CDC*, pages 5453–5458. IEEE, 2012.
- [73] N. Vyas, D. Morwani, R. Zhao, I. Shapira, D. Brandfonbrener, L. Janson, and S. M. Kakade. SOAP: Improving and stabilizing Shampoo using Adam for language modeling. In *ICLR*, 2025.
- [74] J. Wang and G. Joshi. Cooperative SGD: A unified framework for the design and analysis of local-update SGD algorithms. *J. Mach. Learn. Res.*, 22(213):1–50, 2021.
- [75] J. Wang, F. Yu, X. Chen, and L. Zhao. ADMM for efficient deep learning with global convergence. In *Proc. ACM SIGKDD Int. Conf. Knowl. Discov. Data Min.*, pages 111–119, 2019.
- [76] O. Wang, S. Zhou, and G. Y. Li. New environment adaptation with few shots for OFDM receiver and mmwave beamforming. *arXiv preprint arXiv:2310.12343*, 2023.
- [77] J. Weng, H. Chen, D. Yan, K. You, A. Duburcq, M. Zhang, Y. Su, H. Su, and J. Zhu. Tianshou: A highly modularized deep reinforcement learning library. *J. Mach. Learn. Res.*, 23(267):1–6, 2022.
- [78] X. Xie, P. Zhou, H. Li, Z. Lin, and S. Yan. Adan: Adaptive Nesterov momentum algorithm for faster optimizing deep models. *IEEE Trans. Pattern Anal. Mach. Intell.*, 46(12):1–13, 2024.
- [79] K. Xu, S. Zhou, and G. Y. Li. Federated reinforcement learning for resource allocation in V2X networks. *IEEE J. Sel. Topics Signal Process.*, 2024.
- [80] Y. Yang, J. Sun, H. Li, and Z. Xu. ADMM-CSNet: A deep learning approach for image compressive sensing. *IEEE Trans. Pattern Anal. Mach. Intell.*, 42(3):521–538, 2018.
- [81] M. Ye, X. Fang, B. Du, P. C. Yuen, and D. Tao. Heterogeneous federated learning: State-of-the-art and research challenges. *ACM Comput. Surv.*, 56(3):1–44, 2023.
- [82] H. Yong, Y. Sun, and L. Zhang. A general regret bound of preconditioned gradient method for DNN training. In *CVPR*, pages 7866–7875. IEEE, 2023.
- [83] Y. You, I. Gitman, and B. Ginsburg. Scaling SGD batch size to 32k for imagenet training. *arXiv:1708.03888*, 2017.

- [84] Y. You, J. Li, S. Reddi, J. Hseu, S. Kumar, S. Bhojanapalli, X. Song, J. Demmel, K. Keutzer, and C.-J. Hsieh. Large batch optimization for deep learning: Training BERT in 76 minutes. In *ICLR*, 2020.
- [85] H. Yu, S. Yang, and S. Zhu. Parallel restarted SGD with faster convergence and less communication: Demystifying why model averaging works for deep learning. In *AAAI*, volume 33, pages 5693–5700, 2019.
- [86] M. Zaheer, S. Reddi, D. Sachan, S. Kale, and S. Kumar. Adaptive methods for nonconvex optimization. *NeurIPS*, 31, 2018.
- [87] M. D. Zeiler. Adadelta: An adaptive learning rate method. *arXiv:1212.5701*, 2012.
- [88] J. Zeng, S.-B. Lin, Y. Yao, and D.-X. Zhou. On ADMM in deep learning: Convergence and saturation-avoidance. *J. Mach. Learn. Res.*, 22(1):9024–9090, 2021.
- [89] Y. Zeng, Z. Wang, J. Bai, and X. Shen. An accelerated stochastic ADMM for nonconvex and nonsmooth finite-sum optimization. *Automatica*, 163:111554, 2024.
- [90] C. Zhang, J. Cheng, and Q. Li. An optimal control view of LoRA and binary controller design for vision transformers. In *ECCV*, pages 144–160. Springer, 2024.
- [91] T. Zhang, V. Kishore, F. Wu, K. Q. Weinberger, and Y. Artzi. Bertscore: Evaluating text generation with bert. In *ICLR*, 2020.
- [92] X. Zhang, M. Hong, S. Dhople, W. Yin, and Y. Liu. FedPD: A federated learning framework with adaptivity to non-iid data. *IEEE Tran. Signal Process.*, 69:6055–6070, 2021.
- [93] Y. Zhang, C. Chen, Z. Li, T. Ding, C. Wu, D. P. Kingma, Y. Ye, Z.-Q. Luo, and R. Sun. Adam-mini: Use fewer learning rates to gain more. In *ICLR*, 2025.
- [94] W. Zhong and J. Kwok. Fast stochastic alternating direction method of multipliers. In *ICML*, pages 46–54, 2014.
- [95] S. Zhou and G. Y. Li. Federated learning via inexact ADMM. *IEEE Trans. Pattern. Anal. Mach. Intell.*, 45(8):9699–9708, 2023.
- [96] S. Zhou and G. Y. Li. FedGiA: An efficient hybrid algorithm for federated learning. *IEEE Trans. Signal Process.*, 71:1493–1508, 2023.
- [97] J. Zhuang, T. Tang, Y. Ding, S. C. Tatikonda, N. Dvornik, X. Papademetris, and J. Duncan. Adabelief optimizer: Adapting stepsizes by the belief in observed gradients. *NeurIPS*, 33:18795–18806, 2020.
- [98] M. Zinkevich, M. Weimer, L. Li, and A. Smola. Parallelized stochastic gradient descent. *NeurIPS*, 23, 2010.
- [99] F. Zou, L. Shen, Z. Jie, W. Zhang, and W. Liu. A sufficient condition for convergences of Adam and RMSProp. In *CVPR*, pages 11127–11135. IEEE, 2019.

A Appendix: Extended Data

A.1 Hyperparameters of All Experiments

Table 5: Hyperparameters of SISA and NSISA in the numerical experiments.

	model	σ_i^0	ρ_i	γ_i	μ	λ	E	m	n	$ \mathcal{D}_{ij} $
VMs Training	ResNet-18	0.005	2e3/3	1	0	0	303	4	4	8e4
	ViT-B-16	0.005	2e4	1	0	0	380	4	4	8e4
	AlexNet	0.050	2e4	1	0	0	380	4	4	8e4
	DenseNet-121	0.005	2e3/3	1	0	0	303	4	4	8e4
VMs Testing	ResNet-34	0.10	5e3	$\gamma_\ell(0.80, 15)^*$	5e-5	0	200	4	390	32
	VGG-11	4.50	3e4	$\gamma_\ell(0.90, 10)$	2.5e-4	4e-4	200	4	390	32
	DenseNet-121	0.8	2e3	$\gamma_\ell(0.25, 50)$	5e-4	5e-5	200	4	390	64
	ResNet-18	1.00	2e3	1	1e-2	5e-6	100	4	5000	64
LLMs	GPT(124M)	0.01	2.5e4	γ_ℓ^*	0	0	80	4	4	62
	GPT(335M)	0.01	1e4	γ_ℓ	0	0	150	4	4	62
	GPT2 [†]	8e1	1e2	γ_ℓ	0	0	-	4	-	16
RLMs	Ant	5.0	2e4	γ_ℓ	0	0	100	4	112	64
	Humanoid	0.1	1e5	γ_ℓ	0	0	100	4	112	64
	Half-Cheetah	0.5	2e2	γ_ℓ	0	0	100	4	117	64
	Pendulum	0.5	2e2	γ_ℓ	0	0	100	4	117	64
GANs	WGAN	1e-1	1e3	1	0	5e-5	100	4	937	16
	WGAN-GP	5e-5	2e2	1	0	1e-4	100	2	937	32
RNNs	1 layer	0.04	4e2	1	1.2e-6	0	200	4	663	5
	2 layer	0.01	2e2/3	1	1.2e-6	0	200	4	663	5
	3 layer	0.01	2e2/3	1	1.2e-6	0	200	4	663	5

* $\gamma_\ell(t, s) = t$ if ℓ is a multiple of sn and $= 1$ otherwise.

* $\gamma_\ell = 1 - \frac{1}{E - \lfloor \ell/n \rfloor}$, where E is the number of total epochs and $\lfloor a \rfloor$ is the floor of a .

[†] Hyperparameters are set for NSISA. The remaining is set for SISA.

A.2 Effect of Key Parameters

We consider a simple example where the function f is a least squares loss, namely,

$$f(\mathbf{w}; \mathbf{x}) = \frac{1}{2}(\langle \mathbf{w}, \mathbf{a} \rangle - b)^2,$$

where $\mathbf{x} = (\mathbf{a}, b)$. The data generation process follows that in [95]. We use a setup with $m = 32$ batches, $\mu = \lambda = 0$, and $\mathbf{w} \in \mathbb{R}^{100}$. Our experiments reveal that parameters (σ_i^0, γ_i) significantly influence the performance of the proposed algorithm. For simplicity, we set $\sigma_i^0 = \sigma^0$ and $\gamma_i^0 = \gamma$

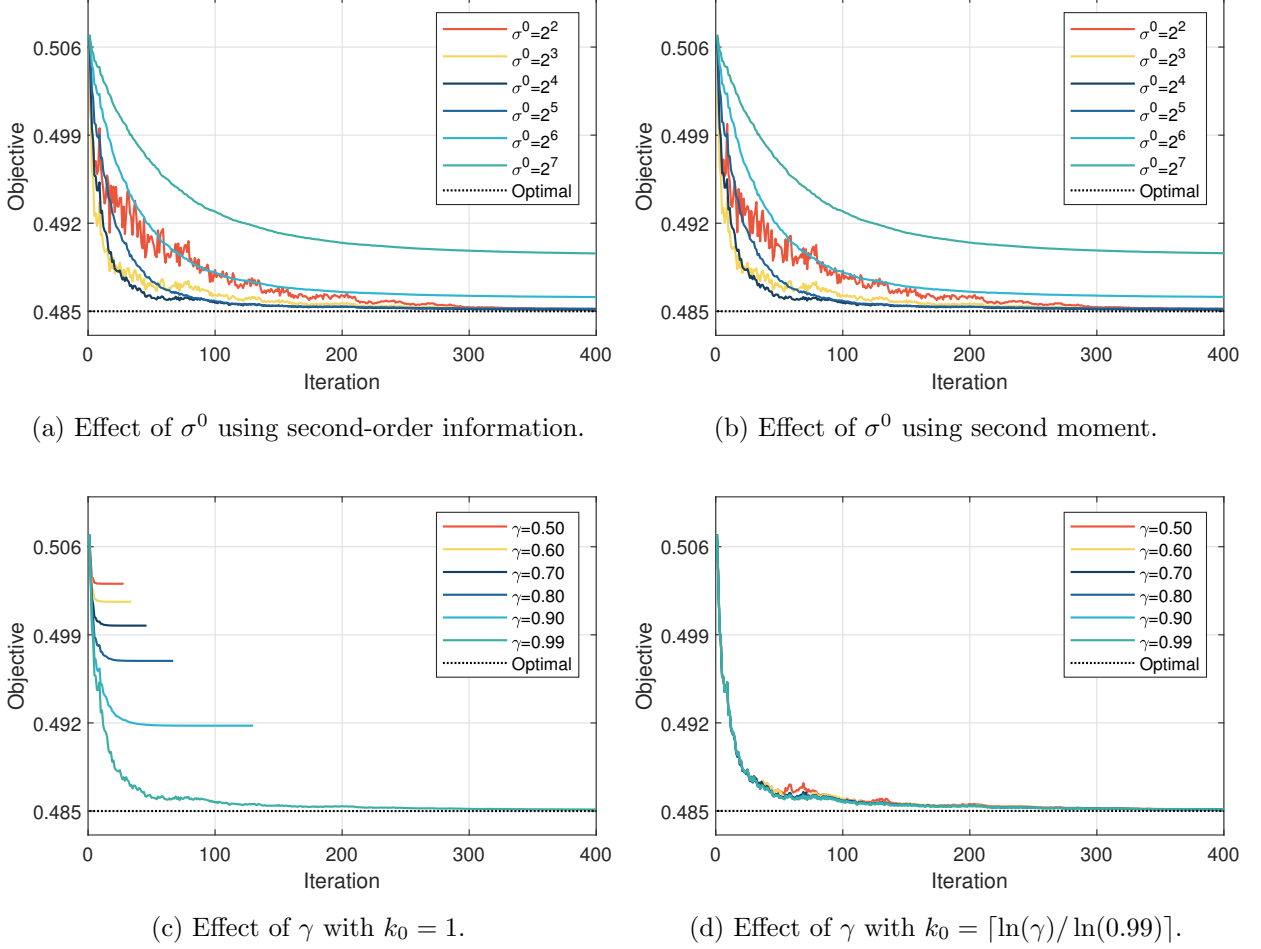


Figure 4: Effect of σ^0 and γ .

for all $i \in [m]$. According to Algorithms 1-3, update rule $\sigma_i^\ell = \sigma^0 \gamma^{-\ell}$ may result in rapid growth of σ_i^ℓ if γ is far from 1 (e.g., $\gamma \in (0, 0.9]$). However, empirical evidence suggests that updating σ_i^ℓ at every iteration is not always ideal. Instead, updating it every few iterations (e.g., when ℓ is a multiple of k_0) can lead to improved performance. We will demonstrate this in the sequel.

a) Effect of σ^0 . To examine the effect of σ^0 , we fix $\gamma = 0.99$, vary $\sigma^0 \in \{2^2, 2^3, \dots, 2^7\}$, and set $k_0 = 1$, meaning σ_i^ℓ is updated at every iteration, namely $k_0 = 1$. We implement PISA using both second-order information (i.e., (4.1)) and second moment estimation (i.e., Scheme III in (4.4)) to construct \mathbf{Q}_i^ℓ . Note that when second moment is used, PISA reduces to SISA (i.e., Algorithm 2). The results are shown in Figures 4a and 4b. When $\sigma^0 = 2^2$, the objective curves fluctuate significantly during the first 100 iterations but eventually converge to the optimal value. With $\sigma^0 = 2^4$ or 2^5 , the convergence is more stable and reaches the optimum efficiently. However, for $\sigma^0 > 2^6$, the curves are very smooth but fail to reach the optimal value.

These findings provide practical guidance for tuning σ^0 . Specifically, one can initialize the algorithm with a moderately small value of σ^0 , depending on the task. If the algorithm exhibits persistent oscillations or divergence within the first few hundred iterations, it may be beneficial to restart with a larger σ^0 . This tuning process can be repeated until a steadily decreasing objective is observed.

b) Effect of γ . To study the effect of γ , we fix $\sigma^0 = 2^4$ and alter $\gamma \in \{0.5, 0.6, 0.7, 0.8, 0.9, 0.99\}$. We employ SISA to solve the problem with updating σ_i^ℓ at every iteration. As shown in Figure 4c, the algorithm achieves the optimal value only when $\gamma = 0.99$. This result is expected since the update rule, $\sigma_i^\ell = \sigma^0 \gamma^{-\ell}$, causes σ_i^ℓ to grow rapidly for $\gamma \leq 0.99$, forcing premature convergence to suboptimal values. Interestingly, Theorem 3.2 (specifically, Equation (3.10)) suggests that smaller γ leads to faster convergence in theory, which is indeed supported by the results in Figure 4c. However, this theoretical speedup comes at the cost of solution quality.

To moderate the effect of fast-growing σ_i^ℓ , we recommend updating it less frequently, such as only when ℓ is a multiple of k_0 . However, determining a suitable k_0 for a given γ is nontrivial. Nevertheless, a practical strategy is to choose k_0 such that the cumulative decay rate over K iterations matches that of $\gamma = 0.99$, namely,

$$0.99^K = \gamma^{K/k_0} \quad \implies \quad k_0 = \left\lceil \frac{\ln(\gamma)}{\ln(0.99)} \right\rceil. \quad (\text{A.1})$$

For example, $k_0 = 69, 36, 11, 1$ when $\gamma = 0.5, 0.7, 0.9, 0.99$, respectively. Using this strategy, we run SISA with updating σ_i^ℓ only when ℓ is a multiple of $k_0 = \lceil \ln(\gamma)/\ln(0.99) \rceil$. As shown in Figure 4d, all curves closely follow the same trajectory and converge to the optimal value, confirming the effectiveness of the proposed approach for choosing k_0 based on (A.1).

Overall, according to Table 5, a recommended range for $(\sigma_i^0, \gamma_i^0, k_0)$ for each $i \in [m]$ can be $\sigma_i^0 \in \{0.005, 0.01, 0.05, 0.1, 0.5\}$, $\gamma_i^0 \in \{0.99, 0.995, 0.999\}$, and k_0 chosen as (A.1).

A.3 Classification by VMs

We perform classification tasks using ImageNet [34] and evaluate the performance by reporting the convergence speed. To validate this, we adopt a large-batch training strategy, which provides more stable gradient estimates and reduces variance in parameter updates. All experimental settings follow the official implementations of widely used model architectures on the ImageNet dataset¹. We compare SISA with five optimizers: Adam, AdamW, AdaBelief, Lamb, and SGD-M [60] on training four VMs: ViT [13], AlexNet [34], ResNet [24], and DenseNet [28]. To ensure fair comparison, all models are trained using identical training strategies and hyperparameters, such as batch size and weight decay. The only exception is the learning rate (which plays a role analogous to σ and ρ in SISA), which is tuned for each optimizer to achieve comparable performance. Figure 5 illustrates the training loss over epochs, and SISA consistently achieves the fastest convergence and maintains the lowest training loss.

A.4 Training LLMs

We compare SISA and AdamW to train two GPT2 models with 124M and 335M parameters [57], following the experimental setup and hyperparameter configurations outlined in [71]. To prevent overfitting, we terminate SISA at the 25th epoch at which the testing loss begins to rise. To evaluate performance, we report both the training and testing loss, as well as the semantic similarity

¹<https://github.com/pytorch/examples/tree/main/imagenet>

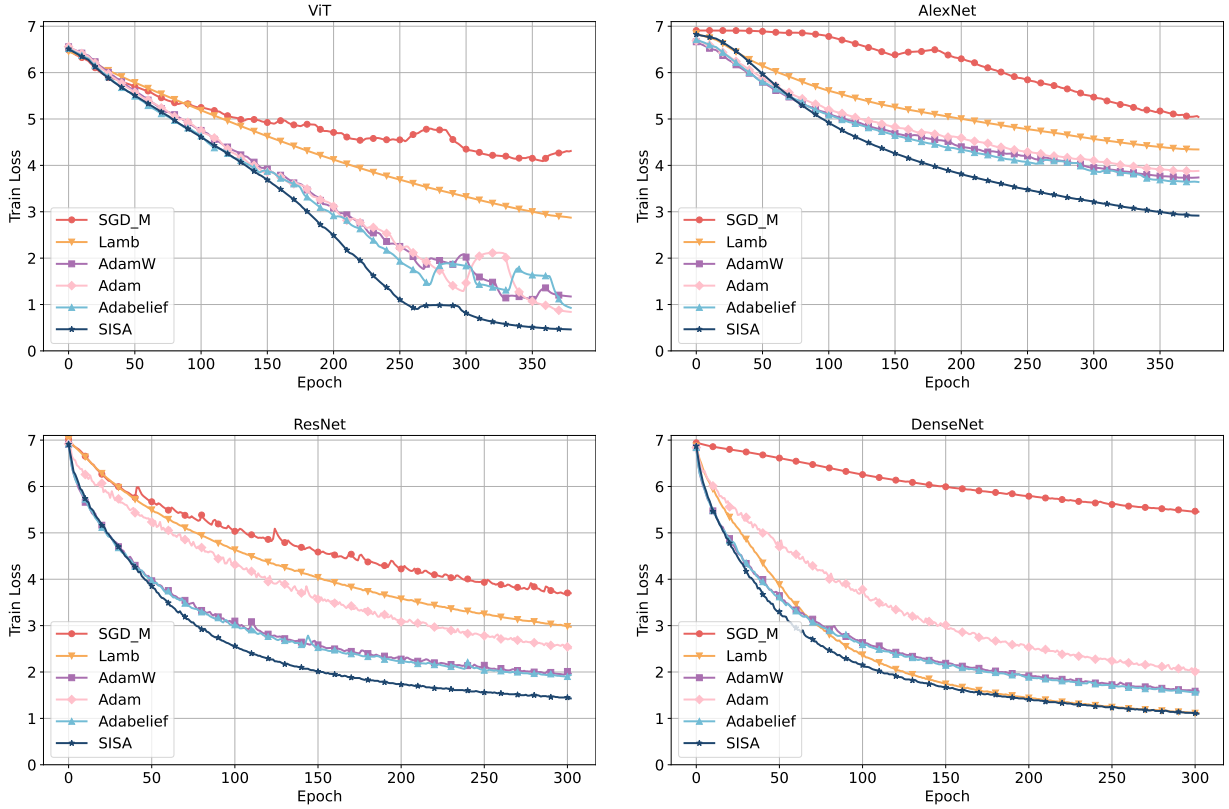


Figure 5: Training loss over epochs for four VMs on ImageNet.

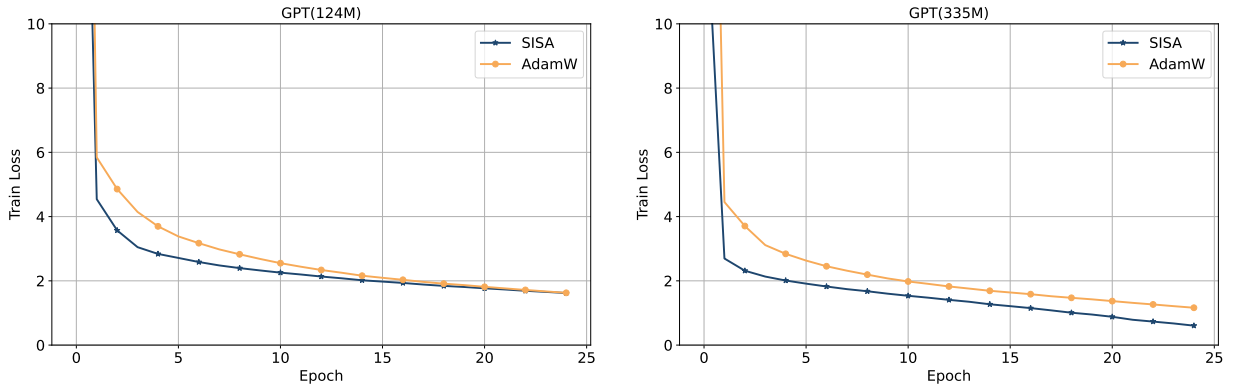


Figure 6: Training loss over epochs for fine-tuning GPT2.

[91]. It noted that lower training and testing loss and higher semantic similarity indicate better performance. Semantic similarity is computed using BERTScore [91], which compares the contextual word embeddings from a pre-trained BERT model to capture the deeper meaning of two texts, rather than relying on exact word matches, and calculates an overall similarity score. By incorporating semantic similarity alongside testing loss, we provide a more comprehensive evaluation of the generated recipes, considering both token-level accuracy and logical coherence. The training process over 25 epochs is shown in Figure 6, where SISA consistently demonstrates faster convergence. Moreover, as illustrated in Table 6, SISA outperforms AdamW in both testing loss and semantic similarity during the early stages of training.

Table 6: Testing loss and semantic similarity for GPT2.

	Epoch	Testing Loss			Semantic Similarity(%)		
		2	5	15	2	5	15
GPT2(124M)	AdamW	5.20	3.45	2.30	82.16	84.30	84.73
	SISA	3.69	2.73	2.17	83.15	84.36	84.82
GPT2(335M)	AdamW	3.62	2.73	1.95	83.17	84.50	84.19
	SISA	2.31	2.04	1.93	84.76	85.24	84.84

Table 7: Memory Overhead (MiB) with Different Optimizers.

	NSISA	Adam	Muon	Shampoo	SOAP	Adam-mini
GPT2-Nano	22,998	22,996	22,998	24,336	26,432	22,996
GPT2-Medium	50,580	50,658	47,860	54,794	58,812	47,548
GPT2-XL	55,126	53,128	50,657	68,146	93,630	50,658

Table 7 reports the memory overhead (in MiB) for different optimizers. Note that the batch size for GPT2-Medium is 16, whereas for GPT2-XL it is 4, with four steps of gradient accumulation. This explains why some optimizers exhibit similar memory overhead for GPT2-Medium and GPT2-XL. We also acknowledge that certain algorithms, such as the one proposed in [90], are specifically designed to reduce memory usage. However, we do not include them in our comparison due to the lack of publicly available implementations. Despite incurring higher memory overhead than some baseline methods, NSISA consistently achieves lower validation loss in less wall-clock time for both the GPT2-Medium and GPT2-XL configurations, as shown in Figure 2.

A.5 Games reward by RLMs

In this subsection, we employ SISA to train RLMs, specifically focusing on two popular algorithms: Proximal Policy Optimization (PPO) and Advantage Actor-Critic (A2C) [15], which are Adam-based approaches. Therefore, we can directly substitute Adam with SISA in PPO and A2C to derive PPO-SISA and A2C-SISA, without requiring additional modification. We refer to the default configurations as PPO-Adam and A2C-Adam. We evaluate these algorithms on four continuous control tasks/games simulated in MuJoCo [69], a widely-used physics engine. The environments for the four tasks are Ant, Humanoid, Half-Cheetah, and Inverted Double Pendulum.

In each test, agents are rewarded at every step based on their actions. Following standard evaluation procedures, we run each task with the same random seeds and assess performance over 10 episodes every 30,000 steps. All experiments are conducted using the Tianshou framework [77] with its default hyperparameters as the baseline. The results are shown in Figure 7, where the solid line represents the average rewards and the shaded region indicates the standard deviation over episodes. Across all four games, SISA outperforms the Adam-based algorithms, achieving higher rewards.

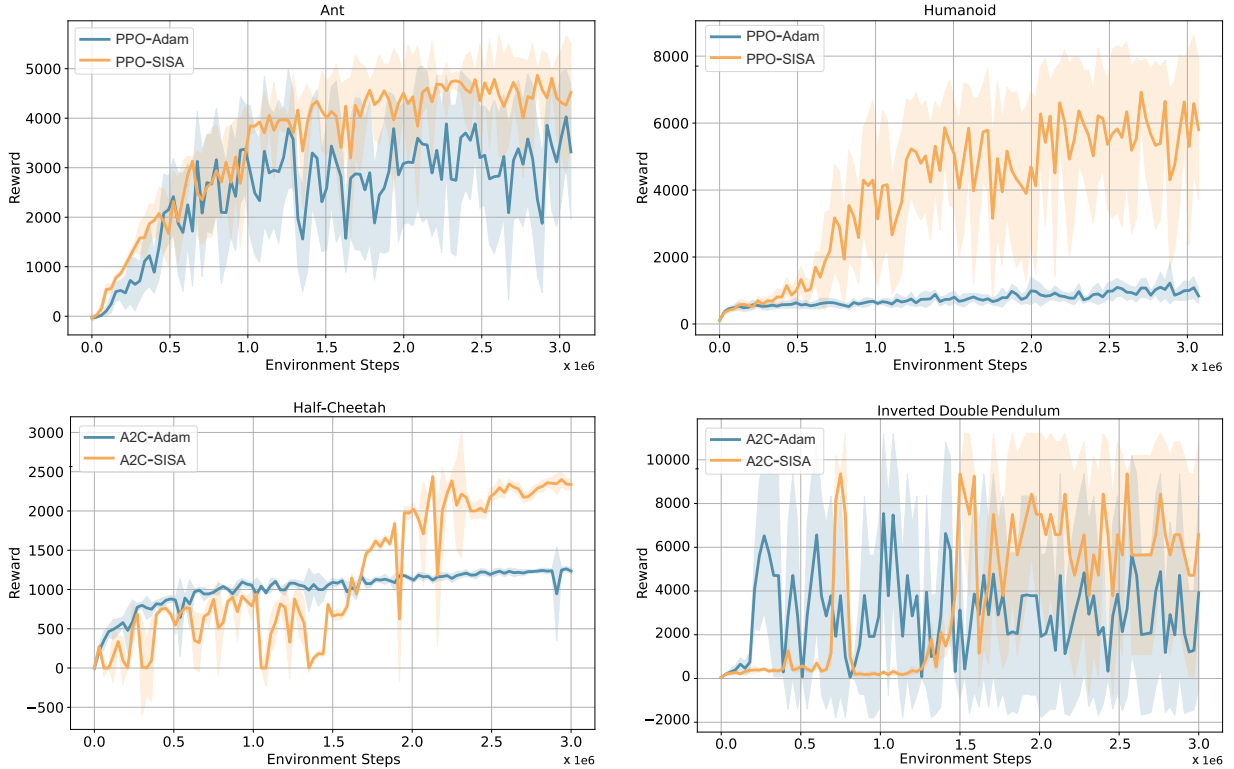


Figure 7: Rewards over steps for RLMs under four environments.

A.6 Text prediction with RNNs

We extend our experiments to natural language processing tasks by applying SISA to long short-term memory (LSTM) networks [21], one of the most widely used RNNs. We adopt the same experimental setup and default hyperparameter configurations as in [97] since the provided code offers a broader range of baseline comparisons. Model performance is evaluated on the Penn TreeBank dataset [45], with perplexity scores reported on the testing dataset. As shown in Table 8, SISA consistently achieves the lowest perplexity across all three LSTM models, demonstrating its effectiveness in improving RNNs performance.

Table 8: Testing perplexity on Penn Treebank for 1, 2, 3-layer LSTM.

	SISA	SGD-M	AdaBound	Adam	Radam	MSVAG	AdamW	AdaBelief	Yogi	Padam
	[60]	[44]	[31]	[41]	[4]	[43]	[97]	[86]	[9]	
1-layer	84.27	85.70	84.73	85.90*	86.50*	84.85	88.39	84.47	86.37	94.46*
2-layer	66.23	67.32	67.43	67.30*	72.30*	68.82*	72.80*	66.70	71.64	89.77*
3-layer	61.06	63.91	63.72	65.02*	70.00*	64.32*	69.90*	61.20	67.69	95.10*

* and * are reported in [78] and [97]. Lower values indicate better performance.

B Appendix: Supplementary Information

In this section, we prove the proof of all theorems in the main context, before the main results, we first present some useful facts.

B.1 Useful facts

- For any $\mathbf{x}, \mathbf{z}, \mathbf{w}$, and \mathbf{v} , and $t > 0$,

$$\begin{aligned} \langle \mathbf{w}, \mathbf{v} \rangle &\leq \frac{t}{2} \|\mathbf{w}\|^2 + \frac{1}{2t} \|\mathbf{v}\|^2 \\ \|\mathbf{w} + \mathbf{v}\|^2 &\leq (1+t) \|\mathbf{w}\|^2 + \left(1 + \frac{1}{t}\right) \|\mathbf{v}\|^2, \\ \langle \mathbf{x} - \mathbf{z}, \mathbf{w} - \mathbf{v} \rangle &\leq \frac{1}{2} \|\mathbf{x} - \mathbf{v}\|^2 - \frac{1}{2} \|\mathbf{x} - \mathbf{w}\|^2 + \frac{1}{2} \|\mathbf{z} - \mathbf{w}\|^2 - \frac{1}{2} \|\mathbf{z} - \mathbf{v}\|^2. \end{aligned} \quad (\text{B.1})$$

- By update (2.9), it follows

$$0 = \sum_{i=1}^m \alpha_i \left[-\boldsymbol{\pi}_i^\ell - \sigma_i^\ell (\mathbf{w}_i^\ell - \mathbf{w}^{\ell+1}) \right] + \lambda \mathbf{w}^{\ell+1}. \quad (\text{B.2})$$

- By update (2.13), it follows

$$\begin{aligned} 0 &= \boldsymbol{\pi}_i^\ell + \mathbf{g}_i^{\ell+1} + \left(\sigma_i^{\ell+1} \mathbf{I} + \rho_i \mathbf{Q}_i^{\ell+1} \right) \Delta \bar{\mathbf{w}}_i^{\ell+1} \\ &\stackrel{(2.14)}{=} \boldsymbol{\pi}_i^{\ell+1} + \mathbf{g}_i^{\ell+1} + \rho_i \mathbf{Q}_i^{\ell+1} \Delta \bar{\mathbf{w}}_i^{\ell+1}. \end{aligned} \quad (\text{B.3})$$

- The choice, $\eta_i \mathbf{I} \succeq \mathbf{Q}_i^{\ell+1} \succeq 0$, of $\mathbf{Q}_i^{\ell+1}$ indicates

$$\left\| \mathbf{Q}_i^{\ell+1} \right\| \leq \eta_i, \quad \forall i \in [m]. \quad (\text{B.4})$$

- We note that the range of γ_i is

$$\frac{3}{4} \leq \gamma_i < 1, \quad \forall i \in [m]. \quad (\text{B.5})$$

Together with (3.4), one can check the following order,

$$\sigma_i^{\ell+1} > \sigma_i^\ell > \sigma_i^0 \geq \sigma^0 \geq 8 \max_{i \in [m]} \left\{ \sigma, \rho_i \eta_i, r_i, \delta^{-2}, \varepsilon_i(2\delta) \right\}, \quad \forall i \in [m], \forall \ell \geq 1. \quad (\text{B.6})$$

Furthermore, for any $\ell \geq 0$,

$$\frac{\varepsilon_i(2\delta)}{\sigma_i^\ell} \stackrel{(2.12)}{=} \frac{\varepsilon_i(2\delta) \gamma_i^\ell}{\sigma_i^0} \stackrel{(B.6)}{\leq} \frac{\gamma_i^\ell}{8} = \frac{\gamma_i^\ell - \gamma_i^{\ell+1}}{8(1 - \gamma_i)}. \quad (\text{B.7})$$

- By letting $\mathbf{P}_i^{\ell+1} := (\sigma_i^{\ell+1} - \sigma_i^\ell) \mathbf{I} + \rho_i \mathbf{Q}_i^{\ell+1}$, it follows

$$\|\mathbf{P}_i^{\ell+1}\| \stackrel{(B.4)}{\leq} \sigma_i^{\ell+1} - \sigma_i^\ell + \rho_i \eta_i \stackrel{(2.12, B.6)}{\leq} \left(\frac{1}{\gamma_i} - 1 + \frac{1}{8} \right) \sigma_i^\ell \stackrel{(B.5)}{\leq} \frac{\sigma_i^\ell}{2}. \quad (\text{B.8})$$

- Let $(\mathbf{w}^*, \mathbf{W}^*)$ be the optimal solution to (2.3). Since F^* is the optimal function value and is lower bounded, for any $\mathbf{w} = \mathbf{w}_i, i \in [m]$, it holds

$$\begin{aligned} -\infty < F^* &= \sum_{i=1}^m \alpha_i F_i(\mathbf{w}_i^*) + \frac{\lambda}{2} \|\mathbf{w}^*\|^2 \leq \sum_{i=1}^m \alpha_i F_i(\mathbf{w}_i) + \frac{\lambda}{2} \|\mathbf{w}\|^2 \\ &= \sum_{i=1}^m \alpha_i F_i(\mathbf{w}) + \frac{\lambda}{2} \|\mathbf{w}\|^2 = F(\mathbf{w}) + \frac{\lambda}{2} \|\mathbf{w}\|^2. \end{aligned} \quad (\text{B.9})$$

- To make these notation in (3.5) well-defined when $\ell = 0$, we let $\mathbf{w}^{-1} = \mathbf{w}^0$, $\mathbf{w}_i^{-1} = \mathbf{w}_i^0$, $\boldsymbol{\pi}_i^{-1} = \boldsymbol{\pi}_i^0$, and $\mathbf{g}_i^0 = \nabla F_i(\mathbf{w}^0)$ for any $i \in [m]$.

B.2 Key lemmas

Lemma B.1. Under Assumption 3.1, for any $\mathbf{w}, \mathbf{v} \in \mathbb{N}(2\delta)$ and any $\mathcal{B}_i \subseteq \mathcal{D}_i$,

$$\begin{aligned} \|\nabla F_i(\mathbf{w}; \mathcal{B}_i) - \nabla F_i(\mathbf{v}; \mathcal{B}_i)\| &\leq \frac{\sigma_i^\ell}{8} \|\mathbf{w} - \mathbf{v}\|, \quad \forall i \in [m], \forall \ell \geq 0, \\ F_i(\mathbf{w}) - F_i(\mathbf{v}) &\leq \langle \nabla F_i(\mathbf{u}), \mathbf{w} - \mathbf{v} \rangle + \frac{\sigma_i^\ell}{16} \|\mathbf{w} - \mathbf{v}\|^2, \quad \forall i \in [m], \forall \ell \geq 0, \end{aligned} \quad (\text{B.10})$$

where $\mathbf{u} = \mathbf{w}$ or $\mathbf{u} = \mathbf{v}$.

Proof. The Lipschitz continuity of $\nabla f(\cdot; \mathbf{x}_t)$ with $c(\mathbf{x}_t) > 0$ on $\mathbb{N}(2\delta)$ and $r_i = \max_{\mathbf{x}_t \in \mathcal{D}_i} c(\mathbf{x}_t) + \mu - \lambda$ imply that, for any $\mathcal{B}_i \subseteq \mathcal{D}_i$,

$$\begin{aligned} \left\| \nabla F_i(\mathbf{w}; \mathcal{B}_i) - \nabla F_i(\mathbf{v}; \mathcal{B}_i) \right\| &\stackrel{(2.4)}{=} \left\| \nabla H_i(\mathbf{w}; \mathcal{B}_i) - \nabla H_i(\mathbf{v}; \mathcal{B}_i) + (\mu - \lambda)(\mathbf{w} - \mathbf{v}) \right\| \\ &\leq \left\| \frac{1}{|\mathcal{B}_i|} \sum_{\mathbf{x}_t \in \mathcal{B}_i} (\nabla f(\mathbf{w}; \mathbf{x}_t) - \nabla f(\mathbf{v}; \mathbf{x}_t)) \right\| + (\mu - \lambda) \|\mathbf{w} - \mathbf{v}\| \\ &\leq \frac{1}{|\mathcal{B}_i|} \sum_{\mathbf{x}_t \in \mathcal{B}_i} c(\mathbf{x}_t) \|\mathbf{w} - \mathbf{v}\| + (\mu - \lambda) \|\mathbf{w} - \mathbf{v}\| \\ &= r_i \|\mathbf{w} - \mathbf{v}\| \stackrel{(B.6)}{\leq} \frac{\sigma_i^\ell}{8} \|\mathbf{w} - \mathbf{v}\| \end{aligned} \quad (\text{B.11})$$

It follows from [96, Eq. (37)] and the above condition that for $\mathbf{u} = \mathbf{w}$ or $\mathbf{u} = \mathbf{v}$,

$$\begin{aligned} F_i(\mathbf{w}) - F_i(\mathbf{v}) &\leq \langle \nabla F_i(\mathbf{u}), \mathbf{w} - \mathbf{v} \rangle + \frac{r_i}{2} \|\mathbf{w} - \mathbf{v}\|^2 \\ &\stackrel{(B.6)}{\leq} \langle \nabla F_i(\mathbf{u}), \mathbf{w} - \mathbf{v} \rangle + \frac{\sigma_i^\ell}{16} \|\mathbf{w} - \mathbf{v}\|^2, \end{aligned}$$

showing the desired result. \square

Lemma B.2. Let $\{(\mathbf{w}^\ell, \mathbf{W}^\ell, \boldsymbol{\Pi}^\ell)\}$ be the sequence generated by Algorithm 1 with $\boldsymbol{\sigma}^0$ chosen as (3.4). Under Assumption 3.1, if $\mathbf{w}^\ell, \mathbf{w}_i^\ell \in \mathbb{N}(\delta)$ for any $i \in [m]$, then $\mathbf{w}^{\ell+1}, \mathbf{w}_i^{\ell+1} \in \mathbb{N}(2\delta)$ and

$$\tilde{\mathcal{L}}^{\ell+1} \geq \mathcal{L}^{\ell+1} \geq \sum_{i=1}^m \alpha_i \left[F_i(\mathbf{w}^{\ell+1}) + \frac{\sigma}{2} \|\Delta \bar{\mathbf{w}}_i^{\ell+1}\|^2 - 1 + \frac{\lambda}{2} \|\mathbf{w}^{\ell+1}\|^2 \right] \geq F^* - 1. \quad (\text{B.12})$$

Proof. By $\mathbf{w}^\ell, \mathbf{w}_i^\ell \in \mathbb{N}(\delta)$, we obtain

$$\rho_i \|\mathbf{Q}_i^\ell \Delta \bar{\mathbf{w}}_i^\ell\| \stackrel{\text{(B.6)}}{\leq} \frac{\sigma_i^\ell}{8} (\|\mathbf{w}^\ell\| + \|\mathbf{w}_i^\ell\|) \leq \frac{\sigma_i^\ell \delta}{4},$$

and the following bound,

$$\frac{\|\mathbf{g}_i^\ell\|}{\sigma_i^\ell} \stackrel{\text{(3.1)}}{\leq} \frac{\sqrt{\varepsilon_i(\delta)}}{8\sigma_i^\ell} \stackrel{\text{(3.1)}}{\leq} \frac{\sqrt{\varepsilon_i(2\delta)}}{8\sigma_i^\ell} \stackrel{\text{(B.6)}}{\leq} \frac{1}{8\sqrt{8\sigma_i^\ell}} \stackrel{\text{(B.6)}}{\leq} \frac{\delta}{64}.$$

Let $t_\ell := \sum_{i=1}^m \alpha_i \sigma_i^\ell + \lambda$. Based on the above conditions, we obtain

$$\begin{aligned} \|\mathbf{w}^{\ell+1}\| &= \frac{1}{t_\ell} \left\| \sum_{i=1}^m \alpha_i \left(\sigma_i^\ell \mathbf{w}_i^\ell + \boldsymbol{\pi}_i^\ell \right) \right\| \\ &\stackrel{\text{(B.3)}}{=} \frac{1}{t_\ell} \left\| \sum_{i=1}^m \alpha_i \left(\sigma_i^\ell \mathbf{w}_i^\ell - \rho_i \mathbf{Q}_i^\ell \Delta \bar{\mathbf{w}}_i^\ell - \mathbf{g}_i^\ell \right) \right\| \\ &= \frac{1}{t_\ell} \left\| \sum_{i=1}^m \alpha_i \left((\sigma_i^\ell - \rho_i \mathbf{Q}_i^\ell) \mathbf{w}_i^\ell - \rho_i \mathbf{Q}_i^\ell \mathbf{w}^\ell - \mathbf{g}_i^\ell \right) \right\| \\ &\leq \frac{1}{t_\ell} \sum_{i=1}^m \alpha_i \left(\sigma_i^\ell \|\mathbf{w}_i^\ell\| + \rho_i \eta_i \|\mathbf{w}^\ell\| + \|\mathbf{g}_i^\ell\| \right) \\ &\leq \delta + \frac{\delta}{8} + \frac{\delta}{64} \leq \frac{73\delta}{64}, \end{aligned}$$

thereby leading to $\mathbf{w}^{\ell+1} \in \mathbb{N}(2\delta)$ and thus

$$\left\| \Delta \mathbf{g}_i^{\ell+1} \right\|^2 \stackrel{\text{(3.1)}}{\leq} \frac{\varepsilon_i(2\delta)}{64}. \quad (\text{B.13})$$

Now we estimate $\mathbf{w}_i^{\ell+1}$ by

$$\begin{aligned} \|\mathbf{w}_i^{\ell+1}\| &\stackrel{\text{(B.3)}}{=} \left\| \left(\sigma_i^{\ell+1} \mathbf{I} + \rho_i \mathbf{Q}_i^{\ell+1} \right)^{-1} \left(-\boldsymbol{\pi}_i^{\ell+1} - \mathbf{g}_i^{\ell+1} \right) + \mathbf{w}_i^{\ell+1} \right\| \\ &\stackrel{\text{(B.3)}}{=} \left\| \left(\sigma_i^{\ell+1} \mathbf{I} + \rho_i \mathbf{Q}_i^{\ell+1} \right)^{-1} \left(\rho_i \mathbf{Q}_i^\ell \Delta \bar{\mathbf{w}}_i^\ell + \mathbf{g}_i^\ell - \mathbf{g}_i^{\ell+1} \right) + \mathbf{w}_i^{\ell+1} \right\| \\ &\stackrel{\text{(B.3)}}{\leq} \frac{1}{\sigma_i^{\ell+1}} \left(\|\rho_i \mathbf{Q}_i^\ell \Delta \bar{\mathbf{w}}_i^\ell\| + \|\mathbf{g}_i^\ell\| + \|\mathbf{g}_i^{\ell+1}\| \right) + \|\mathbf{w}_i^{\ell+1}\| \\ &\stackrel{\text{(B.3)}}{\leq} \frac{\delta}{4} + \frac{2\delta}{64} + \frac{73\delta}{64} \leq 2\delta. \end{aligned}$$

One can verify that

$$\begin{aligned} \left\langle -\mathbf{g}_i^{\ell+1}, \Delta \bar{\mathbf{w}}_i^{\ell+1} \right\rangle &\stackrel{\text{(B.3)}}{=} \left\langle \boldsymbol{\pi}_i^{\ell+1} + \rho_i \mathbf{Q}_i^{\ell+1} \Delta \bar{\mathbf{w}}_i^{\ell+1}, \Delta \bar{\mathbf{w}}_i^{\ell+1} \right\rangle \\ &\stackrel{\text{(B.4)}}{\leq} \left\langle \boldsymbol{\pi}_i^{\ell+1}, \Delta \bar{\mathbf{w}}_i^{\ell+1} \right\rangle + \rho_i \eta_i \left\| \Delta \bar{\mathbf{w}}_i^{\ell+1} \right\|^2 \\ &\stackrel{\text{(B.6)}}{\leq} \left\langle \boldsymbol{\pi}_i^{\ell+1}, \Delta \bar{\mathbf{w}}_i^{\ell+1} \right\rangle + \frac{\sigma_i^{\ell+1}}{8} \left\| \Delta \bar{\mathbf{w}}_i^{\ell+1} \right\|^2, \\ \left\langle \Delta \mathbf{g}_i^{\ell+1}, \Delta \bar{\mathbf{w}}_i^{\ell+1} \right\rangle &\stackrel{\text{(B.1)}}{\leq} \frac{\sigma_i^{\ell+1}}{16} \left\| \Delta \bar{\mathbf{w}}_i^{\ell+1} \right\|^2 + \frac{4}{\sigma_i^{\ell+1}} \left\| \Delta \mathbf{g}_i^{\ell+1} \right\|^2. \end{aligned} \quad (\text{B.14})$$

These two conditions and $\mathbf{w}^{\ell+1}, \mathbf{w}_i^{\ell+1} \in \mathbb{N}(2\delta)$ lead to

$$\begin{aligned}
F_i(\mathbf{w}^{\ell+1}) &\stackrel{(B.10)}{\leq} F_i(\mathbf{w}_i^{\ell+1}) + \left\langle -\nabla F_i(\mathbf{w}^{\ell+1}), \Delta \bar{\mathbf{w}}_i^{\ell+1} \right\rangle + \frac{\sigma_i^{\ell+1}}{16} \left\| \Delta \bar{\mathbf{w}}_i^{\ell+1} \right\|^2 \\
&\stackrel{(3.5)}{=} F_i(\mathbf{w}_i^{\ell+1}) + \left\langle \Delta \mathbf{g}_i^{\ell+1} - \mathbf{g}_i^{\ell+1}, \Delta \bar{\mathbf{w}}_i^{\ell+1} \right\rangle + \frac{\sigma_i^{\ell+1}}{16} \left\| \Delta \bar{\mathbf{w}}_i^{\ell+1} \right\|^2 \\
&\leq F_i(\mathbf{w}_i^{\ell+1}) + \left\langle \boldsymbol{\pi}_i^{\ell+1}, \Delta \bar{\mathbf{w}}_i^{\ell+1} \right\rangle + \frac{\sigma_i^{\ell+1}}{4} \left\| \Delta \bar{\mathbf{w}}_i^{\ell+1} \right\|^2 + \frac{4}{\sigma_i^{\ell+1}} \left\| \Delta \mathbf{g}_i^{\ell+1} \right\|^2,
\end{aligned} \tag{B.15}$$

thereby bringing out

$$\begin{aligned}
\tilde{\mathcal{L}}^{\ell+1} &\stackrel{(3.7)}{\geq} \mathcal{L}^{\ell+1} \stackrel{(2.6)}{=} \sum_{i=1}^m \alpha_i \left[F_i(\mathbf{w}_i^{\ell+1}) + \left\langle \boldsymbol{\pi}_i^{\ell+1}, \Delta \bar{\mathbf{w}}_i^{\ell+1} \right\rangle + \frac{\sigma_i^{\ell+1}}{2} \left\| \Delta \bar{\mathbf{w}}_i^{\ell+1} \right\|^2 + \frac{\lambda}{2} \left\| \mathbf{w}^{\ell+1} \right\|^2 \right] \\
&\stackrel{(B.15)}{\geq} \sum_{i=1}^m \alpha_i \left[F_i(\mathbf{w}_i^{\ell+1}) + \frac{\sigma_i^{\ell+1}}{4} \left\| \Delta \bar{\mathbf{w}}_i^{\ell+1} \right\|^2 - \frac{4}{\sigma_i^{\ell+1}} \left\| \Delta \mathbf{g}_i^{\ell+1} \right\|^2 + \frac{\lambda}{2} \left\| \mathbf{w}^{\ell+1} \right\|^2 \right] \\
&\stackrel{(B.13)}{\geq} \sum_{i=1}^m \alpha_i \left[F_i(\mathbf{w}_i^{\ell+1}) + \frac{\sigma_i^0}{4} \left\| \Delta \bar{\mathbf{w}}_i^{\ell+1} \right\|^2 - \frac{\varepsilon_i(2\delta)}{16\sigma_i^{\ell+1}} + \frac{\lambda}{2} \left\| \mathbf{w}^{\ell+1} \right\|^2 \right] \\
&\stackrel{(B.6)}{\geq} \sum_{i=1}^m \alpha_i \left[F_i(\mathbf{w}_i^{\ell+1}) + \frac{\sigma}{2} \left\| \Delta \bar{\mathbf{w}}_i^{\ell+1} \right\|^2 - 1 + \frac{\lambda}{2} \left\| \mathbf{w}^{\ell+1} \right\|^2 \right] \\
&\stackrel{(B.9)}{\geq} F^* - 1,
\end{aligned}$$

showing the desired result. \square

Lemma B.3. *Let $\{(\mathbf{w}^\ell, \mathbf{W}^\ell, \boldsymbol{\Pi}^\ell)\}$ be the sequence generated by Algorithm 1 with $\boldsymbol{\sigma}^0$ chosen as (3.4). Under Assumption 3.1, for any $i \in [m]$ and any $\ell \geq 0$, if $\mathbf{w}^\ell, \mathbf{w}_i^\ell \in \mathbb{N}(\delta)$ then*

$$\left\| \Delta \boldsymbol{\pi}_i^{\ell+1} \right\|^2 \leq \frac{\varepsilon_i(2\delta)}{6} + \frac{16\varphi_i^{\ell+1}}{3}, \tag{B.16}$$

where $\varphi_i^{\ell+1}$ is defined by

$$\varphi_i^{\ell+1} := \left\| \rho_i \mathbf{Q}_i^\ell \Delta \bar{\mathbf{w}}_i^\ell \right\|^2 - \left\| \rho_i \mathbf{Q}_i^{\ell+1} \Delta \bar{\mathbf{w}}_i^{\ell+1} \right\|^2. \tag{B.17}$$

Proof. First, it follows from $\mathbf{w}^\ell, \mathbf{w}_i^\ell \in \mathbb{N}(\delta)$ and (B.12) that $\mathbf{w}^{\ell+1}, \mathbf{w}_i^{\ell+1} \in \mathbb{N}(2\delta)$, resulting in

$$\left\| \mathbf{g}_i^{\ell+1} - \mathbf{g}_i^\ell \right\|^2 \leq 2 \left\| \mathbf{g}_i^{\ell+1} \right\|^2 + 2 \left\| \mathbf{g}_i^\ell \right\|^2 \leq \frac{\varepsilon_i(2\delta)}{16}. \tag{B.18}$$

Moreover, one can check that

$$\begin{aligned}
\left\| \rho_i \mathbf{Q}_i^{\ell+1} \Delta \bar{\mathbf{w}}_i^{\ell+1} \right\|^2 + \left\| \rho_i \mathbf{Q}_i^\ell \Delta \bar{\mathbf{w}}_i^\ell \right\|^2 &= \varphi_i^{\ell+1} + 2 \left\| \rho_i \mathbf{Q}_i^{\ell+1} \Delta \bar{\mathbf{w}}_i^{\ell+1} \right\|^2 \\
&\stackrel{(B.4)}{\leq} \varphi_i^{\ell+1} + \frac{2\rho_i^2 \eta_i^2}{(\sigma_i^{\ell+1})^2} \left\| \Delta \boldsymbol{\pi}_i^{\ell+1} \right\|^2 \\
&\stackrel{(B.6)}{\leq} \varphi_i^{\ell+1} + \frac{1}{32} \left\| \Delta \boldsymbol{\pi}_i^{\ell+1} \right\|^2,
\end{aligned}$$

which further results in

$$\begin{aligned}
\left\| \Delta \boldsymbol{\pi}_i^{\ell+1} \right\|^2 &\stackrel{\text{(B.3)}}{=} \left\| \mathbf{g}_i^{\ell+1} - \mathbf{g}_i^\ell + \rho_i \mathbf{Q}_i^{\ell+1} \Delta \bar{\mathbf{w}}_i^{\ell+1} - \rho_i \mathbf{Q}_i^\ell \Delta \bar{\mathbf{w}}_i^\ell \right\|^2 \\
&\stackrel{\text{(B.1)}}{\leq} 2 \left\| \mathbf{g}_i^{\ell+1} - \mathbf{g}_i^\ell \right\|^2 + 4 \left\| \rho_i \mathbf{Q}_i^{\ell+1} \Delta \bar{\mathbf{w}}_i^{\ell+1} \right\|^2 + 4 \left\| \rho_i \mathbf{Q}_i^\ell \Delta \bar{\mathbf{w}}_i^\ell \right\|^2 \\
&\stackrel{\text{(B.18)}}{\leq} \frac{\varepsilon_i(2\delta)}{8} + \frac{1}{8} \left\| \Delta \boldsymbol{\pi}_i^{\ell+1} \right\|^2 + 4\varphi_i^{\ell+1}.
\end{aligned}$$

This enables showing (B.16). \square

B.3 Proof of Lemma 3.2

Proof. We decompose

$$\mathcal{L}^{\ell+1} - \mathcal{L}^\ell = G_0 + G_1 + G_2 + G_3,$$

where G_0, G_1, G_2 , and G_3 are defined by

$$\begin{aligned}
G_0 &:= \mathcal{L} \left(\mathbf{w}^{\ell+1}, \mathbf{W}^{\ell+1}, \boldsymbol{\Pi}^{\ell+1}; \boldsymbol{\sigma}^{\ell+1} \right) - \mathcal{L} \left(\mathbf{w}^{\ell+1}, \mathbf{W}^{\ell+1}, \boldsymbol{\Pi}^{\ell+1}; \boldsymbol{\sigma}^\ell \right), \\
G_1 &:= \mathcal{L} \left(\mathbf{w}^{\ell+1}, \mathbf{W}^{\ell+1}, \boldsymbol{\Pi}^{\ell+1}; \boldsymbol{\sigma}^\ell \right) - \mathcal{L} \left(\mathbf{w}^{\ell+1}, \mathbf{W}^{\ell+1}, \boldsymbol{\Pi}^\ell; \boldsymbol{\sigma}^\ell \right), \\
G_2 &:= \mathcal{L} \left(\mathbf{w}^{\ell+1}, \mathbf{W}^{\ell+1}, \boldsymbol{\Pi}^\ell; \boldsymbol{\sigma}^\ell \right) - \mathcal{L} \left(\mathbf{w}^{\ell+1}, \mathbf{W}^\ell, \boldsymbol{\Pi}^\ell; \boldsymbol{\sigma}^\ell \right), \\
G_3 &:= \mathcal{L} \left(\mathbf{w}^{\ell+1}, \mathbf{W}^\ell, \boldsymbol{\Pi}^\ell; \boldsymbol{\sigma}^\ell \right) - \mathcal{L} \left(\mathbf{w}^\ell, \mathbf{W}^\ell, \boldsymbol{\Pi}^\ell; \boldsymbol{\sigma}^\ell \right).
\end{aligned} \tag{B.19}$$

We prove the results by induction.

Part 1: $\ell = 0$. Since $\mathbf{w}_i^0 = \mathbf{w}^0 = 0$ for any $i \in [m]$, we have that

$$\mathbf{w}^0 \in \mathbb{N}(\delta), \quad \mathbf{w}_i^0 \in \mathbb{N}(\delta), \quad \forall i \in [m]. \tag{B.20}$$

For G_0 , it follows that

$$G_0 = \sum_{i=1}^m \frac{\alpha_i(\sigma_i^1 - \sigma_i^0)}{2} \|\Delta \bar{\mathbf{w}}_i^1\|^2 \stackrel{\text{(2.12;2.14)}}{=} \sum_{i=1}^m \alpha_i \left[\frac{1}{2\sigma_i^1} - \frac{\gamma_i^2}{2\sigma_i^0} \right] \|\Delta \boldsymbol{\pi}_i^1\|^2.$$

For G_1 , we have

$$G_1 = \sum_{i=1}^m \alpha_i \langle \boldsymbol{\pi}_i^1 - \boldsymbol{\pi}_i^0, \mathbf{w}_i^1 - \mathbf{w}^1 \rangle \stackrel{\text{(2.14)}}{=} \sum_{i=1}^m \frac{\alpha_i}{\sigma_i^1} \|\Delta \boldsymbol{\pi}_i^1\|^2.$$

For G_2 , it follows from $\mathbf{w}^0, \mathbf{w}_i^0 \in \mathbb{N}(\delta)$ and (B.12) that $\mathbf{w}^1, \mathbf{w}_i^1 \in \mathbb{N}(2\delta)$, resulting in

$$\begin{aligned}
\langle \nabla F_i(\mathbf{w}_i^1) - \mathbf{g}_i^1, \Delta \mathbf{w}_i^1 \rangle &\stackrel{\text{(B.1)}}{\leq} \frac{4}{\sigma_i^0} \|\nabla F_i(\mathbf{w}_i^1) - \mathbf{g}_i^1\|^2 + \frac{\sigma_i^0}{16} \|\Delta \mathbf{w}_i^1\|^2 \\
&\stackrel{\text{(3.1)}}{\leq} \frac{\varepsilon_i(2\delta)}{4\sigma_i^0} + \frac{\sigma_i^0}{16} \|\Delta \mathbf{w}_i^1\|^2.
\end{aligned} \tag{B.21}$$

This further contributes to

$$\begin{aligned}
F_i(\mathbf{w}_i^1) - F_i(\mathbf{w}_i^0) &\stackrel{(B.10)}{\leq} \langle \nabla F_i(\mathbf{w}_i^1), \Delta \mathbf{w}_i^0 \rangle + \frac{\sigma_i^0}{16} \|\Delta \mathbf{w}_i^1\|^2 \\
&= \langle \nabla F_i(\mathbf{w}_i^1) - \mathbf{g}_i^1, \Delta \mathbf{w}_i^1 \rangle + \langle \mathbf{g}_i^1, \Delta \mathbf{w}_i^1 \rangle + \frac{\sigma_i^0}{16} \|\Delta \mathbf{w}_i^1\|^2 \\
&\stackrel{(B.21)}{\leq} \langle \mathbf{g}_i^1, \Delta \mathbf{w}_i^1 \rangle + \frac{\sigma_i^0}{8} \|\Delta \mathbf{w}_i^1\|^2 + \frac{\varepsilon_i(2\delta)}{4\sigma_i^0}.
\end{aligned} \tag{B.22}$$

In addition, one can check that

$$\begin{aligned}
-\langle \mathbf{P}_i^1 \Delta \bar{\mathbf{w}}_i^1, \Delta \mathbf{w}_i^1 \rangle &\stackrel{(B.1)}{\leq} \frac{\sigma_i^0}{8} \|\Delta \mathbf{w}_i^1\|^2 + \frac{2}{\sigma_i^0} \|\mathbf{P}_i^1 \Delta \bar{\mathbf{w}}_i^1\|^2 \\
&\stackrel{(B.8)}{\leq} \frac{\sigma_i^0}{8} \|\Delta \mathbf{w}_i^1\|^2 + \frac{\sigma_i^0}{2} \|\Delta \bar{\mathbf{w}}_i^1\|^2 \\
&\stackrel{(2.14)}{\leq} \frac{\sigma_i^0}{8} \|\Delta \mathbf{w}_i^1\|^2 + \frac{\gamma_i^2}{2\sigma_i^0} \|\Delta \boldsymbol{\pi}_i^1\|^2.
\end{aligned} \tag{B.23}$$

The above facts enable us to derive that

$$\begin{aligned}
p_i &:= L_i(\mathbf{w}^1, \mathbf{w}_i^1, \boldsymbol{\pi}_i^0; \sigma_i^0) - L_i(\mathbf{w}^1, \mathbf{w}_i^0, \boldsymbol{\pi}_i^0; \sigma_i^0) \\
&\stackrel{(2.6)}{=} F_i(\mathbf{w}_i^1) - F_i(\mathbf{w}_i^0) + \langle \boldsymbol{\pi}_i^0 + \sigma_i^0 \Delta \bar{\mathbf{w}}_i^1, \Delta \mathbf{w}_i^1 \rangle - \frac{\sigma_i^0}{2} \|\Delta \mathbf{w}_i^1\|^2 \\
&\stackrel{(B.22)}{\leq} \frac{\varepsilon_i(2\delta)}{4\sigma_i^0} - \frac{3\sigma_i^0}{8} \|\Delta \mathbf{w}_i^1\|^2 + \langle \mathbf{g}_i^1 + \boldsymbol{\pi}_i^0 + \sigma_i^0 \Delta \bar{\mathbf{w}}_i^1, \Delta \mathbf{w}_i^1 \rangle \\
&\stackrel{(B.3)}{=} \frac{\varepsilon_i(2\delta)}{4\sigma_i^0} - \frac{3\sigma_i^0}{8} \|\Delta \mathbf{w}_i^1\|^2 - \langle \mathbf{P}_i^1 \Delta \bar{\mathbf{w}}_i^1, \Delta \mathbf{w}_i^1 \rangle \\
&\stackrel{(B.23)}{\leq} \frac{\varepsilon_i(2\delta)}{4\sigma_i^0} - \frac{\sigma_i^0}{4} \|\Delta \mathbf{w}_i^1\|^2 + \frac{\gamma_i^2}{2\sigma_i^0} \|\Delta \boldsymbol{\pi}_i^1\|^2,
\end{aligned}$$

which immediately leads to

$$G_2 = \sum_{i=1}^m \alpha_i p_i \leq \sum_{i=1}^m \alpha_i \left[\frac{\varepsilon_i(2\delta)}{4\sigma_i^0} - \frac{\sigma_i^0}{4} \|\Delta \mathbf{w}_i^1\|^2 + \frac{\gamma_i^2}{2\sigma_i^0} \|\Delta \boldsymbol{\pi}_i^1\|^2 \right].$$

For G_3 , direct verification leads to

$$\begin{aligned}
G_3 &= \sum_{i=1}^m \alpha_i \left[\langle \boldsymbol{\pi}_i^0, -\Delta \mathbf{w}^1 \rangle + \frac{\sigma_i^0}{2} \|\mathbf{w}_i^0 - \mathbf{w}^1\|^2 - \frac{\sigma_i^0}{2} \|\mathbf{w}_i^0 - \mathbf{w}^0\|^2 \right] + \frac{\lambda}{2} \|\mathbf{w}^1\|^2 - \frac{\lambda}{2} \|\mathbf{w}^0\|^2 \\
&= \sum_{i=1}^m \alpha_i \left[\langle -\boldsymbol{\pi}_i^0 + \sigma_i^0(\mathbf{w}^1 - \mathbf{w}_i^0) + \lambda \mathbf{w}^1, \Delta \mathbf{w}^1 \rangle - \frac{\sigma_i^0 + \lambda}{2} \|\Delta \mathbf{w}^1\|^2 \right] \\
&\stackrel{(B.2)}{=} \sum_{i=1}^m \alpha_i \left[-\frac{\sigma_i^0 + \lambda}{2} \|\Delta \mathbf{w}^1\|^2 \right].
\end{aligned}$$

Overall, the upper bounds of G_0, G_1, G_2 , and G_3 yield that

$$\begin{aligned}
\mathcal{L}^1 - \mathcal{L}^0 &\leq \sum_{i=1}^m \alpha_i \left[\frac{\varepsilon_i(2\delta)}{4\sigma_i^0} - \frac{\sigma_i^0 + 2\lambda}{2} \|\Delta \mathbf{w}^1\|^2 - \frac{\sigma_i^0}{4} \|\Delta \mathbf{w}_i^1\|^2 + \frac{3}{2\sigma_i^0} \|\Delta \boldsymbol{\pi}_i^1\|^2 \right] \\
&\stackrel{(B.16)}{\leq} \sum_{i=1}^m \alpha_i \left[\frac{\varepsilon_i(2\delta)}{2\sigma_i^0} + \frac{8\varphi_i^1}{\sigma_i^0} - \frac{\sigma_i^0 + 2\lambda}{2} \|\Delta \mathbf{w}^1\|^2 - \frac{\sigma_i^0}{4} \|\Delta \mathbf{w}_i^1\|^2 \right] \\
&\stackrel{(B.7)}{\leq} \sum_{i=1}^m \alpha_i \left[\frac{\gamma_i^0 - \gamma_i^1}{16(1 - \gamma_i)} + \frac{8}{\sigma_i^0} \|\rho_i \mathbf{Q}_i^0 \Delta \bar{\mathbf{w}}_i^0\|^2 - \frac{8}{\sigma_i^1} \|\rho_i \mathbf{Q}_i^1 \Delta \bar{\mathbf{w}}_i^1\|^2 \right] \\
&\quad - \sum_{i=1}^m \alpha_i \left[\frac{\sigma_i^0 + 2\lambda}{4} \|\Delta \mathbf{w}^1\|^2 + \frac{\sigma_i^0}{4} \|\Delta \mathbf{w}_i^1\|^2 \right],
\end{aligned} \tag{B.24}$$

sufficing to the following condition, i.e., condition (3.6) with $\ell = 0$,

$$\sum_{i=1}^m \alpha_i \left[\frac{\sigma_i^0 + 2\lambda}{4} \|\Delta \mathbf{w}^1\|^2 + \frac{\sigma_i^0}{4} \|\Delta \mathbf{w}_i^1\|^2 \right] \leq \tilde{\mathcal{L}}^0 - \tilde{\mathcal{L}}^1. \tag{B.25}$$

The initialization in Algorithm 1 implies that $\Delta \bar{\mathbf{w}}_i^0 = 0$, thereby

$$\tilde{\mathcal{L}}^0 = \mathcal{L}^0 + \sum_{i=1}^m \frac{\alpha_i \gamma_i^0}{16(1 - \gamma_i)} \leq F(\mathbf{w}^0) + \frac{1}{16(1 - \gamma)} \stackrel{(B.5)}{\leq} F(\mathbf{w}^0) + \frac{\gamma}{1 - \gamma},$$

which results in

$$\sum_{i=1}^m \alpha_i \left[F_i(\mathbf{w}^1) + \frac{\sigma}{2} \|\Delta \bar{\mathbf{w}}_i^1\|^2 + \frac{\lambda}{2} \|\mathbf{w}^1\|^2 \right] \stackrel{(B.12)}{\leq} \tilde{\mathcal{L}}^1 + 1 \stackrel{(B.25)}{\leq} \tilde{\mathcal{L}}^0 + 1 \leq F(\mathbf{w}^0) + \frac{1}{1 - \gamma}. \tag{B.26}$$

This above condition implies that $(\mathbf{w}^1, \mathbf{W}^1) \in \Omega$ by (3.2), namely,

$$\mathbf{w}^1 \in \mathbb{N}(\delta), \quad \mathbf{w}_i^1 \in \mathbb{N}(\delta), \quad \forall i \in [m],$$

Part 2: $\ell = 1$. Using the above condition and the similar reasoning to show (B.25) enable us to derive (3.6) for $\ell = 1$. Then we can show $\mathbf{w}^1 \in \mathbb{N}(\delta)$ and $\mathbf{w}_i^1 \in \mathbb{N}(\delta)$ for any $i \in [m]$ by using the similar reasoning to prove (B.26).

Part 3: $\ell \geq 2$. Repeating the above process for all $\ell = 2, 3, \dots$ allows us to prove the result. \square

B.4 Proof of Theorem 3.1

Proof. By (3.6) and (B.12), sequence $\{\tilde{\mathcal{L}}^\ell\}$ is non-increasing and lower bounded, so it converges. Taking the limit of both sides of (3.6) yields $\lim_{\ell \rightarrow \infty} \sigma_i^\ell \|\Delta \mathbf{w}^\ell\|^2 = \lim_{\ell \rightarrow \infty} \sigma_i^\ell \|\Delta \mathbf{w}_i^\ell\|^2 = 0$, thereby $\lim_{\ell \rightarrow \infty} \|\Delta \mathbf{w}^\ell\| = \lim_{\ell \rightarrow \infty} \|\Delta \mathbf{w}_i^\ell\| = 0$, and hence $\lim_{\ell \rightarrow \infty} (\tilde{\mathcal{L}}^\ell - \mathcal{L}^\ell) = 0$ by (3.7).

2) Hereafter, we define

$$r = \max_{i \in [m]} r_i, \quad \rho := \max_{i \in [m]} \rho_i, \quad \eta := \max_{i \in [m]} \eta_i, \quad \varepsilon := \max_{i \in [m]} \varepsilon_i(\delta).$$

It follows from Lemma 3.2 that $\mathbf{w}^\ell, \mathbf{w}_i^\ell \in \mathbb{N}(\delta)$ for any $i \in [m]$ and $\ell \geq 0$, thereby

$$\begin{aligned} \|\boldsymbol{\pi}_i^\ell\|^2 &\stackrel{\text{(B.3)}}{=} \|\mathbf{g}_i^\ell + \rho_i \mathbf{Q}_i^\ell \Delta \bar{\mathbf{w}}_i^\ell\|^2 \\ &\stackrel{\text{(B.1)}}{\leq} 5\|\mathbf{g}_i^\ell\|^2 + (5/4)\|\rho_i \mathbf{Q}_i^\ell \Delta \bar{\mathbf{w}}_i^\ell\|^2 \\ &\stackrel{\text{(3.1)}}{\leq} 5\varepsilon/64 + 5(\rho\eta\delta)^2. \end{aligned} \tag{B.27}$$

Hence sequence $\{(\mathbf{w}^\ell, \mathbf{W}^\ell, \boldsymbol{\Pi}^\ell)\}$ is bounded. We note from Lemma 3.2 that for any i and ℓ , it follows $\mathbf{w}^\ell, \mathbf{w}_i^\ell \in \mathbb{N}(\delta)$, thereby

$$\begin{aligned} \|\sigma_i^{\ell+1} \Delta \bar{\mathbf{w}}_i^{\ell+1}\|^2 &\leq \left\| \left(\sigma_i^{\ell+1} \mathbf{I} + \rho_i \mathbf{Q}_i^{\ell+1} \right) \Delta \bar{\mathbf{w}}_i^{\ell+1} \right\|^2 \\ &\stackrel{\text{(B.3)}}{=} \left\| \boldsymbol{\pi}_i^\ell + \mathbf{g}_i^{\ell+1} \right\|^2 \\ &\stackrel{\text{(B.3)}}{\leq} \frac{6}{5} \|\boldsymbol{\pi}_i^\ell\|^2 + 6 \|\mathbf{g}_i^{\ell+1}\|^2 \\ &\stackrel{\text{(B.27)}}{\leq} 6(\rho\eta\delta)^2 + \frac{\varepsilon}{4} =: \varpi^2. \end{aligned} \tag{B.28}$$

Moreover, by letting $t_\ell := \sum_{i=1}^m \alpha_i \sigma_i^\ell$, it follows

$$\begin{aligned} t_\ell \Delta \mathbf{w}^{\ell+1} &\stackrel{\text{(2.9)}}{=} \sum_{i=1}^m \alpha_i \left[\sigma_i^\ell \Delta \bar{\mathbf{w}}_i^\ell + \boldsymbol{\pi}_i^\ell - \lambda \mathbf{w}^{\ell+1} \right] \\ &\stackrel{\text{(B.3)}}{=} \sum_{i=1}^m \alpha_i \left[\left(\sigma_i^\ell - \rho_i \mathbf{Q}_i^\ell \right) \Delta \bar{\mathbf{w}}_i^\ell - \mathbf{g}_i^\ell - \lambda \mathbf{w}^{\ell+1} \right], \end{aligned}$$

which together with $\sum_{i=1}^m \alpha_i = 1$ yields

$$\begin{aligned} t_\ell^2 \|\Delta \mathbf{w}^{\ell+1}\|^2 &\leq \sum_{i=1}^m \alpha_i \left[3 \|\sigma_i^\ell \Delta \bar{\mathbf{w}}_i^\ell\|^2 + 3\|\mathbf{g}_i^\ell\|^2 + 3\lambda^2 \|\mathbf{w}^{\ell+1}\|^2 \right] \\ &\stackrel{\text{(B.28)}}{\leq} \sum_{i=1}^m \alpha_i \left[\left(18(\rho\eta)^2 + 3\lambda^2 \right) \delta^2 + \varepsilon \right] =: c^2. \end{aligned}$$

Since $\gamma = \max_{i \in [m]} \gamma_i$ and $\sigma_i^0 > \sigma$ for any $i \in [m]$ from (3.4), we obtain

$$\|\Delta \mathbf{w}^{\ell+1}\| \leq \frac{c}{t_\ell} = c \left(\sum_{i=1}^m \frac{\alpha_i \sigma_i^0}{\gamma_i^\ell} \right)^{-1} \leq \frac{c\gamma^\ell}{\sigma}. \tag{B.29}$$

For every given $\epsilon > 0$, by letting $K \geq \log_\gamma((1-\gamma)\sigma\epsilon/c)$, for any $s > k > K$, there is

$$\|\mathbf{w}^s - \mathbf{w}^k\| \leq \sum_{\ell=k}^s \|\Delta \mathbf{w}^{\ell+1}\| \leq \sum_{\ell=k}^s \frac{c\gamma^\ell}{\sigma} \leq \frac{c\gamma^k}{\sigma(1-\gamma)} \leq \epsilon,$$

which means $\{\mathbf{w}^\ell\}$ is a Cauchy sequence. Therefore, sequence $\{\mathbf{w}^\ell\}$ converges. By (B.28), we can prove $\lim_{\ell \rightarrow \infty} (\mathbf{w}_i^\ell - \mathbf{w}^\ell) = 0$ and thus sequence $\{\mathbf{w}_i^\ell\}$ converges for each $i \in [m]$. Let \mathbf{w}^∞ be the limit of $\{\mathbf{w}^\ell\}$. We note that \mathbf{w}^ℓ is independent to \mathcal{B}_i^ℓ for each $i \in [m]$ and thus

$$\mathbb{E} \mathbf{g}_i^\ell = \mathbb{E} \nabla F_i(\mathbf{w}^\ell; \mathcal{B}_i^\ell) = \nabla F_i(\mathbf{w}^\ell). \tag{B.30}$$

Recalling (B.3), it follows

$$\begin{aligned}
0 &= \lim_{\ell \rightarrow \infty} \mathbb{E} \left[\boldsymbol{\pi}_i^\ell + \mathbf{g}_i^\ell + \rho_i \mathbf{Q}_i^\ell \Delta \bar{\mathbf{w}}_i^\ell \right] \\
&= \lim_{\ell \rightarrow \infty} \left[\mathbb{E} \boldsymbol{\pi}_i^\ell + \nabla F_i(\mathbf{w}^\ell) \right] \\
&= \lim_{\ell \rightarrow \infty} \left[\mathbb{E} \boldsymbol{\pi}_i^\ell + \nabla F_i(\mathbf{w}^\infty) \right].
\end{aligned}$$

Therefore, sequence $\{\mathbb{E} \boldsymbol{\pi}_i^\ell\}$ converges. \square

B.5 Proof of Theorem 3.2

Proof. It follows from (B.29) that

$$\left\| \mathbf{w}^\ell - \mathbf{w}^\infty \right\| \leq \sum_{k=\ell}^{\infty} \left\| \Delta \mathbf{w}^{k+1} \right\| \leq \sum_{k=\ell}^{\infty} \frac{c\gamma^k}{\sigma} = \frac{c\gamma^\ell}{\sigma(1-\gamma)}.$$

This condition and $\sigma_i^\ell = \sigma_i^0 / \gamma_i^\ell$ further lead to

$$\begin{aligned}
\left\| \mathbf{w}_i^\ell - \mathbf{w}^\infty \right\| &\leq \left\| \Delta \bar{\mathbf{w}}_i^\ell \right\| + \left\| \mathbf{w}^\ell - \mathbf{w}^\infty \right\| \\
&\stackrel{\text{(B.28)}}{\leq} \frac{\varpi \gamma_i^\ell}{\sigma_i^0} + \frac{c\gamma^\ell}{\sigma(1-\gamma)} \\
&\leq \frac{\varpi \gamma^\ell}{\sigma} + \frac{c\gamma^\ell}{\sigma(1-\gamma)}.
\end{aligned}$$

In addition, one can verify that

$$\begin{aligned}
\left\| \mathbb{E} \boldsymbol{\pi}_i^\ell + \nabla F_i(\mathbf{w}^\ell) \right\| &\stackrel{\text{(B.30)}}{=} \left\| \mathbb{E} (\boldsymbol{\pi}_i^\ell + \mathbf{g}_i^\ell) \right\| \stackrel{\text{(B.3)}}{\leq} \left\| \mathbb{E} (\rho_i \mathbf{Q}_i^\ell \Delta \bar{\mathbf{w}}_i^\ell) \right\| \\
&\stackrel{\text{(B.4)}}{\leq} \rho_i \eta_i \mathbb{E} \left\| \Delta \bar{\mathbf{w}}_i^\ell \right\| \stackrel{\text{(B.28)}}{\leq} \frac{\varpi \rho_i \eta_i \gamma_i^\ell}{\sigma_i^0} \stackrel{\text{(B.6)}}{\leq} \frac{\varpi \gamma^\ell}{8}.
\end{aligned}$$

Using this condition, it follows

$$\begin{aligned}
\left\| \mathbb{E} \boldsymbol{\pi}_i^\ell + \nabla F_i(\mathbf{w}^\infty) \right\| &\leq \left\| \mathbb{E} \boldsymbol{\pi}_i^\ell + \nabla F_i(\mathbf{w}^\ell) \right\| + \left\| \nabla F_i(\mathbf{w}^\ell) - \nabla F_i(\mathbf{w}^\infty) \right\| \\
&\stackrel{\text{(B.11)}}{\leq} \frac{\varpi \gamma^\ell}{8} + r \left\| \mathbf{w}^\ell - \mathbf{w}^\infty \right\| \leq \frac{\varpi \gamma^\ell}{8} + \frac{cr\gamma^\ell}{\sigma(1-\gamma)}.
\end{aligned}$$

The above facts enable us to show result (3.9) by letting

$$C_1 := \max \left\{ \frac{\varpi}{\sigma} + \frac{c}{\sigma(1-\gamma)}, \frac{\varpi}{8} + \frac{cr}{\sigma(1-\gamma)} \right\}.$$

Now we prove (3.9). It follows from $\mathbf{w}^\ell \in \mathbb{N}(\delta)$ that

$$\begin{aligned}
& F_\lambda(\mathbf{w}^\ell) - F_\lambda(\mathbf{w}^\infty) \\
&= \sum_{i=1}^m \alpha_i \left[F_i(\mathbf{w}^\ell) + \frac{\lambda}{2} \|\mathbf{w}^\ell\|^2 - F_i(\mathbf{w}^\infty) - \frac{\lambda}{2} \|\mathbf{w}\|^2 \right] \\
&\stackrel{\text{(B.10)}}{\leq} \sum_{i=1}^m \alpha_i \left[\left\langle \nabla F_i(\mathbf{w}^\ell) + \lambda \mathbf{w}^\ell, \mathbf{w}^\ell - \mathbf{w}^\infty \right\rangle + \frac{r_i + \lambda}{2} \|\mathbf{w}^\ell - \mathbf{w}^\infty\|^2 \right] \\
&\leq \sum_{i=1}^m \alpha_i \left[\left(\|\nabla F_i(\mathbf{w}^\ell)\| + \lambda \|\mathbf{w}^\ell\| \right) \|\mathbf{w}^\ell - \mathbf{w}^\infty\| + \frac{r + \lambda}{2} \|\mathbf{w}^\ell - \mathbf{w}^\infty\|^2 \right] \\
&\stackrel{\text{(3.1)}}{\leq} \sum_{i=1}^m \alpha_i \left[\frac{\sqrt{\varepsilon(\delta)} + 8\lambda\delta}{8} \|\mathbf{w}^\ell - \mathbf{w}^\infty\| + \frac{r + \lambda}{2} \|\mathbf{w}^\ell - \mathbf{w}^\infty\|^2 \right] \\
&\leq C_2 \gamma^\ell,
\end{aligned} \tag{B.31}$$

for any $i \in [m]$ and $\ell \geq 0$, where C_2 is a constant satisfying

$$C_2 \geq \frac{\sqrt{\varepsilon(\delta)} C_1 + 8\lambda\delta + 4(r + \lambda) C_1^2}{8}.$$

From (B.28), one can verify

$$\left\| \Delta \bar{\mathbf{w}}_i^{\ell+1} \right\|^2 \leq \frac{\varpi^2}{(\sigma_i^{\ell+1})^2} \leq \frac{\varpi^2 \gamma^{\ell+1}}{\sigma^2}.$$

Then using the above fact, the boundedness of $\{\mathbf{\Pi}^\ell\}$, and (B.31) can also show that $\mathcal{L}^\ell - F_\lambda(\mathbf{w}^\infty)$ and $\tilde{\mathcal{L}}^\ell - F_\lambda(\mathbf{w}^\infty)$ is bounded by $C_2 \gamma^\ell$. The proof is finished. \square